High precision osmium stable isotope measurements by double spike MC-ICP-MS and N-TIMS.

Josefine A.M. Nanne*[a], Marc-Alban Millet[a,b], Kevin W. Burton[a], Chris W. Dale[a], Geoff M. Nowell[a] and Helen M. Williams[a,c]

* Corresponding author. E-mail: j.a.nanne@durham.ac.uk

a. Department of Earth Sciences,
Durham University,
Science Labs, South Road,
Durham DH1 3LE, United Kingdom.

b. *Present address:* School of Earth and Ocean Sciences,
Cardiff University,
Main building, Park Place,
Cardiff CF10 3AT, United Kingdom.

c. *Present address:* Department of Earth Sciences,
The University of Cambridge,
Downing Street,
Cambridge CB2 3EQ, United Kingdom.

ABSTRACT

Osmium stable isotopes provide a new, potentially powerful tool with which to investigate a diverse range of geological processes including planetary formation, ore-genesis and weathering. In this paper, we present a new technique for high precision measurement of osmium (Os) stable isotope ratios by both Multiple-Collector Inductively Coupled Plasma Mass Spectrometry (MC-ICP-MS) and Negative ion Thermal Ionisation Mass Spectrometry (N-TIMS). We use a 188Os-190Os double spike, composed of 61% 188Os and 39% 190Os, to correct for mass dependent fractionation resulting from sample preparation and isotope measurement, with the ideal spike to sample ratio being 55:45. Isotope ratios are expressed as δ190Os which is the per mil deviation in the measured 190Os/188Os ratio relative to isotope reference material DROsS. Repeated analyses of double spiked DROsS for both MC-ICP-MS (n= 80 cycles) and N-TIMS (n= 280 cycles) show that an internal precision of 0.01-0.02 ‰ on δ190Os (2 se) can be attained, with a long-term reproducibility of 0.016 ‰ and 0.029 ‰ (2 sd; n = 91 and 83, respectively). The better reproducibility on MC-ICP-MS than on N-TIMS is, predominantly, due to measurement at higher beam intensities (11-18 V with consumption of ~200 ng natural Os vs. 2-18 V with consumption of 2.3 – 45 ng natural Os, respectively). In addition to stable isotope compositions, our method allows for simultaneous measurement of 187Os/188Os and 186Os/188Os ratios with a precision of <40 ppm (2 se; 80 cycles for MC-ICP-MS and 280 cycles for N-TIMS) and an external reproducibility of 123-268 ppm and 234-361 ppm (2 sd; n= 91 for MC-ICP-MS and n= 83 for N-TIMS), respectively. We demonstrate that a similar precision and reproducibility can be obtained for other pure Os solutions as well as for geological materials. In addition, a range of analytical tests evaluates and demonstrates the robustness of our method with regards to residual matrix effects and interference correction, signal intensity and on-peak zero on MC-ICP-MS, and the effect of oxygen corrections and isobaric interference on N-TIMS. Finally, we report the first Os stable isotope compositions for geological reference materials, including mantle peridotites and chromitites, and one ordinary chondrite.

1. INTRODUCTION

Osmium (Os) has two radiogenic isotopes (^{186}Os and ^{187}Os) and five naturally occurring stable isotopes: ^{184}Os, ^{188}Os, ^{189}Os, ^{190}Os, and ^{192}Os, with relative abundances of 0.02 %, 13.21 %, 16.11 %, 26.21 %, and 40.74 %, respectively. Osmium is a refractory and highly siderophile (Fe-loving) element and is therefore of considerable interest in the study of planetary differentiation and formation of Earth's metallic core. It is also a chalcophile (S-loving) element, and strongly partitions into sulphides. Consequently, Os behaves compatibly during mantle melting, where sulphide remains as a residual phase in the source. Taking advantage of the chemical properties of Os and the differences in behaviour between Re, Pt and Os, the ^{187}Re-^{187}Os and ^{190}Pt-^{186}Os decay systems have become important chronometers and tracers in both high and low-temperature geochemistry [e.g.1, 2]. More specifically, these radiogenic isotope systems have been used to study early solar system dynamics [e.g. 3, 4], planetary differentiation processes [e.g. 5, 6], mantle heterogeneity [e.g. 7, 8], crustal growth and recycling [e.g. 9-11], economic mineralization in ore deposits [e.g. 12], and the nature of weathering processes associated with brief climatic excursions [e.g. 13-15]. However, despite the potential to use stable Os isotopes to investigate these same processes, thus far this system remains unexplored.

A potential limitation for the use of Os stable isotopes in geochemistry is the small range of natural variation expected for high-mass elements. This is compounded by the very low abundance of Os in most terrestrial samples. However, recent advances in mass spectrometry and development of new techniques for stable isotope measurement have led to the discovery of significant and systematic stable isotope fractionation for high-mass stable isotope systems in both high and low-temperature environments[16-22]. This suggests that Os stable isotope variations may be measurable if a suitable high precision analytical method can be developed.

Additional complications that must be addressed in order to successfully measure Os stable isotopes include the non-quantitative recovery of Os during sample processing (typically on 60-80 %[23, 24]) and instrumental mass bias (MC-ICP-MS) or mass fractionation (N-TIMS) during measurement. Such fractionation can be overcome by the use of a double spike (DS) [25]. This approach has been shown to reliably account for mass-dependent stable isotope fractionation that can occur during all steps of sample processing (digestion, chemical separation and mass spectrometry) [18, 26, 27].

In this paper, we present a new method for the measurement of high-precision stable Os isotope ratios using a ^{188}Os-^{190}Os double spike by both plasma source (MC-ICP-MS) and negative thermal ionisation mass spectrometry (N-TIMS). Method development on both machines allows for the analysis of sample materials over a broad range of Os concentrations (>1 ppb) at precisions of 0.01-0.02 ‰ on δ^{190}Os (2 se; 80 cycles for MC-ICP-MS and 280 cycles for N-TIMS). In addition, we show that the method allows for simultaneous collection of stable isotopes and radiogenic isotope ratios, ^{187}Os/^{188}Os and ^{186}Os/^{188}Os, at a precision of <40 ppm (2 se; 80 cycles for MC-ICP-MS and 280 cycles for N-TIMS). We show the robustness, precision and accuracy of our method through a range of analytical tests and

repeated measurements of pure Os solutions and geological materials. Finally, data is presented for a range of geological materials.

2. OSMIUM DOUBLE SPIKE METHODOLOGY

2.1 Osmium Double Spike Design

The double spike (DS) approach requires four stable isotopes that are related to each other by mass-dependent stable isotope fractionation. For Os we can use ^{188}Os, ^{189}Os, ^{190}Os, and ^{192}Os. Departures from mass-dependent fractionation, either due to cosmogenic effects or nucleosynthetic anomalies, have not been detected in terrestrial samples but have been reported for extra-terrestrial materials. Components of carbonaceous chondrites display mass independent Os isotopic anomalies although homogeneity is shown at the bulk meteoritic scale [e.g. 28, 29,30]. Mass independent anomalies at the bulk rock scale have been shown for iron meteorites [e.g. 31] which should be considered when analysing such meteorites.

The DS deconvolution used in this study is based on the geometric iterative resolution method of Siebert et al. (2001)[32]. Measurements were also double checked using an algebraic resolution method used by Millet and Dauphas (2014)[33] and Millet et al. (2016)[34] which yielded identical results. Regardless of the approach, the DS deconvolution consists of resolving the following non-linear equation:

$$R_m = \left[(1-f)R_{standard}(i_x/i_n)^{\alpha} + fR_{spike}\right] * (i_x/i_n)^{\beta}$$

where R_m, $R_{standard}$ and R_{spike} are the measured, standard and spike isotope ratios; i_n is the atomic weight of the normalising isotope (^{188}Os); i_x is the atomic weight of one of the three other isotopes used to resolve the equation which in our method are ^{189}Os, ^{190}Os and ^{192}Os; f is the relative proportion of ^{188}Os originating from the spike in the sample–spike mixture; α is the natural and β the processing and instrumental exponential fractionation factors. In this study, reference material DROsS has been used as standard. All Os stable isotope compositions are thus reported relative to DROsS, as the per mil deviation (‰) of the ^{190}Os/^{188}Os ratios, here after reported as δ^{190}Os:

$$\delta^{190/188}\mathrm{Os}_{\mathrm{DROsS}} = \left(\frac{\frac{^{190}\mathrm{Os}}{^{188}\mathrm{Os}}_{\mathrm{sample}}}{\frac{^{190}\mathrm{Os}}{^{188}\mathrm{Os}}_{\mathrm{DROsS}}} - 1\right) * 1000$$

Radiogenic isotopes ^{186}Os and ^{187}Os are not used in the DS deconvolution. Consequently, the spike proportion, and the geological and analytical fractionation factors resolved within the DS deconvolution can be used to calculate the ^{186}Os/^{188}Os and ^{187}Os/^{188}Os ratios. Osmium concentrations were determined by performing isotope dilution calculations.

The analytical uncertainty on double spike measurements is highly dependent on spike composition and sample-spike mixing proportions. To establish the optimal composition and

proportions for Os, we have modelled the internal precision of a typical MC-ICP-MS measurement following the model of Millet and Dauphas (2014)[33] which takes into account the errors associated to Johnson noise and counting statistics (see ref. 33 for more details). This error model differs from that of Rudge et al. (2009)[35] in that i) errors on the natural fractionation factor (alpha) are calculated on the basis of a constant intensity for the most abundant isotope in the natural Os-DS mixture, rather than calculated based on a constant total Os ion beam and; ii) determination of errors is done through Monte Carlo modelling. In our model, the maximum intensity for the most abundant isotope was set at 6 V. A measurement is assumed to comprise 80 cycles with an integration time of 8.3 seconds per cycle on $10^{11}\,\Omega$ collectors at T=290 K. The model shows that a minimum internal error, of ~0.010 ‰ amu^{-1} (2 se), is acquired when using a 0.6:0.4 ^{188}Os – ^{190}Os mixed spike composition and a 0.55:0.45 spike-sample mixture (Fig. 1). This is close to the optimal double spike composition as calculated by Rudge et al. (2009)[35] of 0.66:0.34 ^{188}Os -^{190}Os for a 0.6:0.4 spike-sample mixture. It is important to note that the 2 se error is <0.020 ‰ amu^{-1} when the sample proportion ranges between 15 % and 81 %. That errors are minimal over a large range of spike-sample mixtures is of great utility when the Os concentration of samples is not well known. A triple spike composition was considered in our calculations but was not found to improve precision.

2.2 Preparation and calibration of ^{188}Os – ^{190}Os double spike

Single ^{188}Os and ^{190}Os isotope spikes were purchased as fine-grained metallic powders from Trace Sciences International. In order to ensure purity of the double spike, the metal powders were individually digested using Carius tubes, followed by extraction and purification as described in section 3.2. Individual spikes were subsequently mixed in calculated optimal proportions and the resulting double spike was diluted with 3 M HCl to desired concentrations.

Calibration of the double spike isotope composition was achieved by measuring a pure standard and pure double spike solution as well as a range of Durham Romil Osmium Standard (DROsS[36, 37])-DS mixtures. Practically, this involves iterative correction for instrumental mass fractionation of the pure DS measurements to generate a putative true DS composition, with an initial estimate provided by the pure DROsS analysis. This putative true DS composition is then fed into the DS deconvolution and used on all DS-DROsS mixtures, ranging from 0.1:0:9 to 09:0.1 mixing proportions. Calibration is considered satisfactory once most mixtures, especially those around the optimum mixture proportions, display a $\delta^{190}Os$ within analytical error of zero. For all these solutions, Carius tubes were used to ensure standard-sample equilibration. Measurements were carried out by MC-ICP-MS with each analysis comprising 220 cycles of 8.39 seconds and were all preceded by on-mass on-peak zero measurement (20 integrations of 8.39 seconds). The isotope composition of the DS and of reference standard DROsS, as used in the calibration and stable isotope calculations, can be found in Table 1.

3. MATERIALS AND SAMPLE PROCESSING

3.1 Materials and samples

Digestion and processing of standards and samples were carried out at Durham University. During the course of this study, we used Romil acids of variable grades (Super Purity Acids and Ultra Purity Acids) with blank levels suitable for the analytical procedure. The nitric acid was purified by sparging with filtered air. Acid dilutions were performed with ultrapure (18.2 MΩ·cm) water.

We use the Durham Romil Osmium Standard (DROsS)[36, 37] as a reference standard. This is an international Os isotope reference material supplied by IAGeo Limited that has been widely distributed [e.g.38, 39] and for which Os isotope ratios have been determined to high precision and accuracy by both MC-ICP-MS[36] and N-TIMS[37]. For method testing, we have also measured three in-house pure Os reference solutions, ROMIL, SpecPure, and OsCaR, which were purchased from Romil Ltd, Alfa Aesar, and provided by A. Poirier (OsCaR). As representative rock samples, we used well-characterized and commonly used reference materials: peridotites UB-N[40] and GP-13[41], and chromitites CHR-Bkg[42, 43] and CHR-Pt+[44]. Reference material GP-13 is an in-house PGE standard prepared at Durham University which has been widely distributed. The other materials, UB-N, CHR-Bkg and CHR-Pt+, are distributed by CRPG-CRNS, Nancy, France. Furthermore, we included an ordinary H-chondrite, ZAG. These samples were chosen to reflect the range of Os concentrations and sample matrices available for study.

3.2 Sample digestion and chemical purification of Os

Samples were digested either by Carius tube (CT)[23, 45] or high-pressure asher (HPA, Anton Paar)[44], with respective maximum of 2.5 g and 2 g powder material per tube. Digestions were performed using inverse aqua regia (1:2; 12 M HCl: 16 M HNO_3) for ≥16 h at temperatures of 230°C in the case of CT and 290-310°C for HPA digestions. The double spike was added to each tube prior to sample digestion. After digestion, the extraction and purification of Os closely followed techniques described by Cohen et al. (1996)[21] and Birck et al. (1997)[22]. Separation of Os from the aqua regia digest solution was achieved by solvent extraction using $CHCl_3$[46]. Osmium was then back-extracted from the chloroform solution using concentrated HBr and subsequently purified using the micro-distillation procedure of Roy-Barman (1993)[47] as described by Birck et al. (1997)[24]. In the case of measurements by MC-ICP-MS, samples were evaporated and chlorified three times using 300 µL of 8 M HCl before being taken up in 3 M HCl to a total Os concentration of ~0.5 µg mL^{-1}. When performing Os analyses by N-TIMS, samples were dried down after microdistillation to approximately 1-2 µL of sample solution and then loaded onto a Pt ribbon filament. Typical total procedural blanks range between 0.01 and 0.10 pg Os which is similar to previous Os studies carried out at Durham University [e.g. 48].

4. MASS SPECTROMETRY

Osmium isotope ratios were measured at Durham University on a ThermoFisher Scientific Neptune MC-ICP-MS[36] and a Triton Plus N-TIMS[37, 39, 49]. The use of both MC-ICP-MS and N-TIMS allowed us to exploit the advantages of the different ionisation sources and provide a means to assess the relative accuracy of each measurement. The overall introduction and ionisation efficiency of MC-ICP-MS is relatively low (~0.08 %[36]) which makes it better suited for analysing large samples and calibrating standards. The advantage of the MC-ICP-MS is that Os is measured as Os^+ which makes the mass spectrum relatively simple and corrections for isobaric interferences relatively straightforward. By contrast, N-TIMS has a much higher ionisation efficiency for Os (1-5 %[37]) which makes it ideal for samples with a low Os abundance or when sample material is limited. However, Os is measured as the tri-oxide ion OsO_3^- which makes the mass spectrum complex and necessitates multiple oxide corrections that add to the overall uncertainty. In both cases, internal errors are presented as the 2 se on $\delta^{190}Os$ of each integration, once passed through a 2 se filter to remove outliers.

4.1 MC-ICP-MS

4.1.1 Instrument set-up and parameters MC-ICP-MS

The Neptune MC-ICP-MS was set-up for static simultaneous collection of all Os isotopes, apart from the least abundant ^{184}Os. We also collected ^{183}W, ^{185}Re, and ^{194}Pt in order to monitor and correct for isobaric interference (Table 2). In this study, interference beam intensities were <0.05 mV for ^{183}W, <0.01 mV for ^{185}Re, and <0.5 mV for ^{194}Pt. Typical instrument operating conditions were similar to those outlined in Nowell et al. (2008)[36]. Sample material was introduced in 3 M HCl using an Elemental Scientific Incorporated (ESI) PFA-50 micro-flow nebuliser and Glass Expansion (GE) micro-cyclonic "Cinnabar" spray-chamber. During typical run conditions, the measured sample uptake rate was ca. 80 µL min^{-1} with a sensitivity of ca. 30 V ppm^{-1}. Measurements were carried out in static mode in 1 block of 80 cycles of 8.389 seconds integration time each. Mass calibration was updated by peak-centering on the centre-cup mass ^{188}Os at the start of each session and checked again at the end. Prior to every sample run, baselines were obtained by on-mass on-peak zero (OPZ) measurements for 20 x 8.389 seconds integrations in clean 3 M HCl. Washouts between sample runs used 3 M HCl acid for at least 5 minutes which resulted in the ^{188}Os beam decreasing below 2 mV (~0.03 % of the typical sample signal). Total analysis time, including OPZ and wash-out, was approximately 15 minutes with consumption of 800 µL sample solution (equivalent to 400 ng total Os in the case of a 0.5 µg mL^{-1} solution).

4.1.2 Data reduction MC-ICP-MS

Following analysis, all raw intensity data were exported and re-processed offline on a cycle-by-cycle basis using an in-house Excel spreadsheet. For MC-ICP-MS analyses, corrections were applied in the following order; baseline subtraction using the OPZ measurements, abundance sensitivity (1 ppm[36]),

isobaric interferences, and DS deconvolution. The abundance sensitivity is assumed to be similar to that determined by Nowell et al. (2008)[36].

4.1.2.1 Effect of beam intensity and on-peak zero

To evaluate the effect of beam size on the accuracy, the main 500 ppb DROsS-DS solution was diluted to various lower concentrations (100 - 5 ppb total Os; Table 3). This resulted in total Os beam intensities varying between 18 V and 0.1 V, with the corresponding ^{188}Os ranging between 6.7 V and 0.005 V. All analyses show Os stable isotope ratios as well as ^{187}Os/^{188}Os within analytical uncertainty of one another (Fig. 2; Table 3). The ^{186}Os/^{188}Os only shows a significant deviation from the reference value when the total Os beam intensity is 0.14 V, corresponding to solutions with concentrations of ~ 5 ppb total Os which equals the consumption of ~4 ng total Os (i.e. natural plus DS) under standard running conditions.

Analyses by MC-ICP-MS at low beam intensities critically rely on the absence of memory effects. The on-peak zero (OPZ), used to account for baseline, can introduce an inaccuracy on the stable isotope composition especially when measuring samples with very distinct isotope composition. The importance of the wash-out and sample to sample memory has been discussed in detail by Nowell et al. (2008)[36]. They show that when certain precautions are taken (e.g., avoid drying out of the spray chamber between sessions, keep standards and samples in the same chemical form), the effect on the Os isotopic composition is negligible and should not prevent the acquisition of high precision data. Considering that the natural variation in stable isotope compositions is expected to be small and the proportion of sample to spike are well matched, the potential of memory effect on the stable isotope ratios can, therefore, assumed to be minimal. In this study, the OPZ of the diluted DROsS solutions display signal intensities between 0.04 % and 0.6 % relative to the peak Os signal (^{188}Os) in the main run. The accuracy of the δ^{190}Os values even at low beam intensities suggests that the OPZ has an insignificant effect on the accuracy at levels up to 0.6 %. For DROsS analyses run at total Os beam intensities of >10 V, OPZ analyses are in general <2 mV and <0.04 % of the peak Os signal. The potential of inaccurate δ^{190}Os values as a result of OPZ analyses can, therefore, be neglected. The fact that OPZ correction is less accurate for ^{186}Os/^{188}Os is partly due to the lower intensities of ^{186}Os relative to all other isotopes involved in the double-spike deconvolution (^{188}Os, ^{189}Os, ^{190}Os and ^{192}Os). The ^{186}Os signal of the OPZ analyses at 0.14 V is 4 % of the main run beam. On-peak zero determination is, therefore, critical for obtaining reliable ^{186}Os/^{188}Os simultaneously with δ^{190}Os by MC-ICP-MS.

It should be noted that the higher ionisation efficiency of the N-TIMS allows for small quantities of Os to be measured at higher intensities. For example, while consumption of 4 ng total Os (5 ppb solution) provides a total Os beam intensities of 0.1 V by MC-ICP-MS, we typically obtain a total Os beam intensity of >1 V for a total Os load of ≥5 ng by N-TIMS. Furthermore, Figure 7 shows that the error is significantly increased when the ^{188}Os beam intensity drops below ~1 V (~2.7 V ^{total}Os) which is

an important consideration to make when small variations in stable isotope composition are expected. We, therefore, recommend that measurements on less than ~100 ng of total Os be performed by N-TIMS.

4.1.2.2 Matrix effects and interference corrections

Potential atomic isobaric inferences on Os isotopes can arise from the incomplete separation of Os from W, Re and Pt. In addition, non-spectral matrix effects can create inaccurate results[50]. To assess if our method can accurately correct for these interferences, we doped double spiked DROsS with a range of elements that are (i) typically found in silicate rocks (Si, Al, Mg, Fe, Ca, Ti, Ni and Cr), (ii) dominant in iron meteorites (Fe, Ni), (iii) platinum group elements (Ru, Rh, Pd, Ir, and Pt), and (iv) trace elements that have direct isobaric interferences on Os (Pt, W and Re). Test solutions were doped at levels ranging from 0.01-10 % of the total Os concentration. Each element was present in x% of the Os abundance, e.g. Si was present at 5% of the Os abundance. All measurements display values that are within analytical uncertainty of undoped DROsS measurements (Fig. 3; Table 3). This illustrates that matrix effects as well as isobaric interferences, even at extreme levels of up to 10 %, can be accurately accounted for. The interference beam intensities monitored for standard solutions as well as geological sample material processed and analysed in this study are all <0.01 % of the total Os concentration and are, therefore, not expected to introduce data inaccuracies.

4.2 N-TIMS

4.2.1 Instrument set-up and parameters

For N-TIMS analyses, sample material was loaded onto Pt single filaments in concentrated HBr or in 3 M HCl when the sample solution was also measured by MC-ICP-MS. After the sample material was dried down on the filament, ~0.5 µL of NaOH-$Ba(OH)_2$ activator was added to enhance ionisation. The amount of Os loaded for this study varied between 2.3 and 45 ng natural Os. Where MC-ICP-MS provides fairly consistent beam intensities for a certain set-up, the intensity that is obtained for a given amount of Os is not directly correlated on N-TIMS, but also depends on the activator and sample loading on the filament. A two-sequence static multi-collection routine was used in order to analyse masses 232 to 242 (Table 2). Masses 241 and 242 are collected to calculate the oxygen isotope compositions (see section 4.2.2). A single analysis consists of 28 blocks, each comprising 10 cycles with 8.389 seconds integration per cycle followed by 3 seconds idle time. Amplifier gain calibrations were performed at the start of each day, although amplifiers were rotated throughout an analysis to cancel out amplifier gains. Baseline measurements and peak centering, using masses 236 and 240, were carried out prior to every run. The presence of interfering PtO_2^-, ReO_3^-, and WO_3^- were quantified by measuring masses 228, 230-233 by ion counter before and after each Faraday measurement for 4-6 cycles with a total analysis time

of 110-160 seconds. During analysis, high purity oxygen (99.6 % purity, supplied by BOC) was bled into the source chamber with the pressure kept constant at ~2.5 x 10^{-7} mbar.

4.2.2 Data reduction N-TIMS

Osmium analyses by N-TIMS are performed using the tri-oxide ion (OsO_3^-) and, therefore, corrections for the effects of variable isobaric oxygen isotope interferences of the heavier oxygen isotopes (^{17}O and ^{18}O) are required. For example, correction for $^{188}Os^{16}O_2{}^{17}O^-$ on $^{189}Os^{16}O_3^-$ at mass 239. In this study, we adopted the method of Luguet et al. (2008)[37] where the O isotope composition is determined in-run for each integration so that any variation throughout an analysis can be accounted for. This is a more accurate approach than using a fixed O isotope composition because the composition has been shown to vary from sample to sample as well as throughout an individual run [e.g. 37, 39, 51, 52]. For comparison, we have also applied the method recommended by Chatterjee and Lassiter (2015)[39] where the O isotopic composition was measured before and after the main run using a separate routine. This routine consisted of the second line as mentioned in Table 2 and data was collected for 10 cycles of 8.389 seconds integrations each. From the 20 cycles, the mean 241/238 and 242/238 values (2 se outlier rejected) were taken as an approximation of the O isotopic composition of the specific run. The collection of masses 241 and 242, which are free from the most abundant Os tri-oxide species ($^{16}O_3$), allows the O isotope compositions to be determined by stripping masses 240, 241 and 242 of the minor tri-oxide interferences, such as $^{189}Os^{16}O^{18}O_2^-$ and $^{190}Os^{17}O_3^-$ for mass 240. This will then provide the signal intensity of only $^{192}Os^{16}O_3^-$, $^{192}Os^{16}O_2{}^{17}O^-$, and $^{192}Os^{16}O_2{}^{18}O^-$ on respective masses 240, 241, and 242. For this first step of oxygen corrections we used the O_{gas} isotope composition as determined by Luguet et al. (2008)[37]. The $^{18}O/^{16}O$ was then calculated from the "stripped" 242/240 ratio and the $^{17}O/^{16}O$ ratio could be determined from the "stripped" 241/240 ratio. However, as discussed in more detail in section 4.2.2.1, in this study $^{17}O/^{16}O$ ratios were inferred using $^{18}O/^{16}O$ ratios. The oxygen correction is described in detail in the Electronic Supplementary Information.

Due to the presence of isobaric Os oxide complexes, additional steps in the data reduction compared to MC-ICP-MS were required. We adopted the following sequence of corrections; abundance sensitivity (0.3 ppm[37]), a preliminary oxide isotope composition correction, PtO_2^- and ReO_3^- interference corrections, a second O isotope composition correction, and double spike deconvolution (see section 4.1.2). The first O interference correction is solely used to correct for O isobaric interferences on PtO_2^-. Subsequently, the PtO_2^- interference corrected $^{184}OsO_3^-$ and $^{186}OsO_3^-$ values were used in the second O correction. For isobaric PtO_2^-, WO_3^- and ReO_3^- interference corrections, the ion counter measurement routines (before and after) were utilized, assuming a linear behaviour throughout the main run. Using a linear extrapolation is a simplistic approach but can be justified by the minor variation in beam intensities between the two SEM runs in combination with the minor influence the interference corrections have on the Os isotopic ratios (see section 4.2.2.2). The abundance sensitivity was assumed to be similar to that determined by Luguet et al. (2008)[37].

331

332 *4.2.2.1 Effect of the oxygen isotopic composition*

333 The accuracy of the deconvolved δ^{190}Os value as well as of the radiogenic isotopic ratios is dependent
334 on the accurate determination of the O isotopic compositions (i.e. $^{17}O/^{16}O$ and $^{18}O/^{16}O$) that are used
335 for O interference corrections.

336 The average $^{18}O/^{16}O$ ratios of individual double spiked DROsS analyses range between
337 0.002007 and 0.002050, a variation of 21 ‰, for analyses with a total Os beam intensity of >1 V. This
338 variation is comparable with that reported by previous Os studies by N-TIMS (e.g. Liu et al., 1998[53] – 30
339 ‰; Luguet et al., 2008[37] – 14 ‰; Chatterjee and Lassiter, 2015[39] – 31 ‰; Chu et al., 2015[54]– 22 ‰). If
340 the $^{18}O/^{16}O$ ratio varies by 21 ‰, and the $^{17}O/^{16}O$ relationship is changed accordingly along a TFL, then
341 the absolute δ^{190}Os value will shift by ±0.11 ‰. For the $^{187}Os/^{188}Os$ and $^{186}Os/^{188}Os$ ratios the resulting
342 absolute shift is about ±20 ppm and ±25 ppm, respectively. It is, therefore, of high importance to
343 determine the specific oxygen isotopic composition of an analysis. When ^{total}Os beam intensities are on
344 average >1 V (>1.3 mV on mass 242), the difference in $^{18}O/^{16}O$ ratios between the first and last 20 cycles
345 of an individual run ranges, apart from two samples at -12 ‰, between +5 ‰ and -7 ‰, and is on
346 average -1.1 ‰. This is similar to the variation observed by Chatterjee and Lassiter (2015)[39]. Larger
347 variations are observed for measurements made at lower beam intensities and the variability appears
348 to be more substantial when samples are run over a longer time period (Fig. 4). If the $^{18}O/^{16}O$ ratio is
349 changed by ±7 ‰, the absolute composition of δ^{190}Os shifts by ±0.025 ‰. The $^{187}Os/^{188}Os$ and
350 $^{186}Os/^{188}Os$ ratios are shifted by ±11 ppm and ±26 ppm, respectively. We, therefore, suggest
351 determining the oxygen isotopic composition for each individual cycle, as this is the only way by which
352 small time scale variations throughout the run can be monitored and controlled.

353 Run-specific $^{17}O/^{16}O$ ratios for each individual cycle can either be measured directly, using
354 mass 241, or can be calculated based on the $^{18}O/^{16}O$ ratios. We will first consider the measured $^{17}O/^{16}O$
355 ratios. For DROsS analyses, the average measured $^{17}O/^{16}O$ ratio was found to display a large variation,
356 of 121 ‰, with values ranging from 0.000369 to 0.000419. When only considering analyses with total
357 beam intensities of >1 V the $^{17}O/^{16}O$ ratios vary between 0.000369 and 0.000395, 66 ‰. Analyses with
358 an anomalously high or low $^{17}O/^{16}O$ ratio yield inaccurate δ^{190}Os values as well as $^{187}Os/^{188}Os$ and
359 $^{186}Os/^{188}Os$ ratios, and show a positive correlation with $^{17}O/^{16}O$ (R^2 of 0.78, 0.78 and 0.76 respectively;
360 Fig. 5a-c). Anomalous values are only obtained for analyses performed at low beam intensities (Fig. 5d-
361 f). In contrast, the measured $^{18}O/^{16}O$ ratios do not show any co-variation with Os isotopic compositions
362 (R^2=0.28) suggesting that the inaccuracy on the Os isotopic compositions is dominantly introduced by
363 the $^{17}O/^{16}O$ ratio. Mass 241 has been measured at very low beam intensities (<5 mV) that are, in general,
364 5.2 times lower than for mass 242. The determination of $^{17}O/^{16}O$ is, therefore, more sensitive to
365 inaccuracies introduced by small variations in the instrument baseline occurring during an analysis.
366 Including more and longer baselines with longer integration times during an analysis would enhance
367 the accuracy of the baseline and potentially improve the measurement of the $^{17}O/^{16}O$ ratio.

Incorporation of 10^{12} Ω or 10^{13} Ω resistors to collect mass 241 and 242 would also be advantageous, although these were not explored in this study.

The inaccuracy introduced by the measured $^{17}O/^{16}O$ ratio can be eliminated by calculating the $^{17}O/^{16}O$ from the measured $^{18}O/^{16}O$ ratio. We will refer to this as the "calculated" $^{17}O/^{16}O$ ratio. Recently, a similar approach has been used for N-TIMS isotope measurements of Mo[52], Ru[55], and W[56]. In this study, we assume that the oxygen isotopic compositions vary as a result of equilibrium mass-dependent isotopic fractionation along a "Terrestrial Fractionation Line" (TFL[57]). For natural samples the relationship between $\delta^{17}O$ and $\delta^{18}O$, when considered in logarithmic space, typically varies between 0.524-0.528 [e.g.58-60]. We have taken an average of the published values, 0.526, which translates to an approximately linear slope of 0.0994 x + 0.000183, where x is $^{18}O/^{16}O$, over a $^{18}O/^{16}O$ interval of 0.002007 to 0.002055, the range in $^{18}O/^{16}O$ as observed for analyses in this study. Figure 6 shows that the measured oxygen compositions of double spiked DROsS analyses with a total Os beam intensity of >2 V closely plot along this line. Details of calculation $^{17}O/^{16}O$ from the measured $^{18}O/^{16}O$ are provided in the supplementary information.

The resulting calculated $^{17}O/^{16}O$ ratios display a much smaller variation of 20 ‰ with values ranging between 0.000383 and 0.000390, and is 10 ‰ when only considering analyses of >1 V. No residual correlation between calculated $^{17}O/^{16}O$ ratios and Os isotopic compositions is observed anymore (Fig. 5a-c). However, with decreasing beam intensities the $\delta^{190}Os$ values display a preferential drift towards heavier values (up to 0.11‰) instead of showing a normal distribution (Fig. 5d). The $^{187}Os/^{188}Os$ and $^{186}Os/^{188}Os$, on the other hand, drift preferentially towards lower values although higher values are observed as well (Fig. 5e,f). When the calculated instead of the measured $^{17}O/^{16}O$ composition is used, the long-term reproducibility of $\delta^{190}Os$ is improved from 0.106 ‰ to 0.046 ‰ (2 sd; *n* = 94), and from 0.059 ‰ to 0.029 ‰ for analyses of >1 V (*n* = 83). For the remainder of this paper, we will only consider analyses with a $^{total}Os$ beam intensity of >1 V, equivalent to, in general, >1.3 mV on mass 242 and >0.35 V on mass 236. The total Os signal intensity obtained for a certain quantity of Os loaded is highly variable, but is typically >1 V for loads of ≥2.3 ng natural Os.

4.2.2.2 Effect of polyatomic interferences

The interference intensities monitored on masses 228, and 230-233 in this study are comparable to those reported by Luguet et al. (2008)[37]. Beam intensities on mass 228 (predominantly $^{196}Pt^{16}O_2^-$) ranged from 12,000 – 1,400,000 cps (counts per second) which relates to a potential $^{196}Pt^{18}O_2^-$ interference of 0.05-6 cps on mass 232 (predominantly $^{184}Os^{16}O_3^-$). For mass 230 (mainly $^{198}Pt^{16}O_2^-$) intensities ranged between 4,000-1,050,000 cps which results in respective interferences of 16-4,300 cps and 0.02-4.4 cps on masses 232 ($^{184}Os^{16}O_3^-$) and 234 ($^{186}Os^{16}O_3^-$). The PtO_2^- interference on mass 234 is negligible, whereas the combined PtO_2^- interferences on mass 232 reached a maximum of 4,306 cps. This represents 2.5 % of the typical total signal at mass 232 which can lower the $^{184}Os/^{188}Os$ substantially

(~30,000 ppm). In this study, mass 234 was only monitored to correct for polyatomic oxygen interferences on the other Os isotopic ratios. Lowering the $^{184}Os/^{188}Os$ by 30,000 ppm results in a minor shift of -2 ppm on the $^{186}Os/^{188}Os$ and has no noticeable effect on the other Os isotopic ratios. The average difference between the two SEM runs, before and after the main run, was 250,000 cps for mass 228 and 135,000 cps for mass 230. Potential within-run variations of this magnitude have no measurable effect on the isotopic ratios. On mass 231, $^{183}WO_3^-$, we obtained intensities of 6-1,000 cps, which produce insignificant interferences on $^{186}Os^{16}O_3^-$ [37, 61]. Mass 233, $^{185}ReO_3^-$, displayed intensities between 3-460 cps but were generally below 300 cps and on average 73 cps. Translated to $^{187}ReO_3^-$ this means <502 cps or 8 µV that interfered on the $^{187}OsO_3^-$. Typically, this quantity equates to a lowering of the $^{187}Os/^{188}Os$ by <100 ppm and on average 38 ppm, which is close to the 2 se of our measurements (40 ppm) but much smaller than the long-term reproducibility (268 ppm; 2 sd). Between the pre- and post SEM runs, the beam intensities on mass 233 generally varied by 33 cps which equates to a shift of ~18 ppm on the $^{187}Os/^{188}Os$. To summarize, polyatomic interferences from PtO_2^-, WO_3^-, and ReO_3^- monitored in this study had no noticeable effect on the stable Os and $^{186}Os/^{188}Os$ isotopic composition, and were minor for $^{187}Os/^{188}Os$ ratios.

5. RESULTS AND DISCUSSION

Results are presented in Tables 4 and 5, and shown in Figures 7-13. All internal errors are quoted as 2 standard error (2 se), whereas short term (i.e. single session) and long-term (i.e. multiple sessions) reproducibilities are given as 2 standard deviations (2 sd).

5.1 Internal precision, external reproducibility and accuracy

5.1.1 Stable osmium isotope ratios by MC-ICP-MS

The internal precision (2 se; $n \leq 80$ cycles, depending on 2 se outlier rejection) on a single $\delta^{190}Os$ MC-ICP-MS analysis is typically between 0.01-0.02 ‰ when ^{188}Os beam intensities range between 7-4 V (~18-11 V $^{total}Os$; Fig. 7). The amount of natural Os consumed is ~200 ng. The observed precision is in good agreement with the theoretical error as calculated in section 2.1 (Fig. 7) suggesting that the model considers all the errors that should be accounted for. Small deviations from the calculated error could have arisen from, for example, variation in the spike – sample proportions, or the number of cycles included. The model considers 80 cycles whereas this can be less for MC-ICP-MS if outliers are rejected. This also explains why the error model for N-TIMS displays lower errors for a given intensity, as 280 cycles were considered for N-TIMS analyses.

Repeated analyses of reference standard solution DROsS, obtained during multiple analytical sessions over a time period of ~22 months, show an external reproducibility on $\delta^{190}Os$ of 0.016 ‰ (2 sd; $n = 91$; Fig. 8; Table 4). The short-term reproducibility of a single analytical session when consuming

~200 ng natural Os at total beam intensities of 11-18 V is 0.014-0.029 ‰ (2 sd; *n* = 2-10). A similar precision and reproducibility is obtained for in-house Os reference solutions ROMIL, SpecPure and OsCaR (Fig. 7 and 9; Table 4). As this study is the first to present stable Os isotope compositions, the accuracy cannot be assessed by measurement of pre-calibrated reference materials. Instead we have performed standard-sample bracketing measurements by MC-ICP-MS using natural (i.e. non DS) reference solutions. Comparison of this technique with the DS method shows that a similar offset between DROsS and the other Os reference solutions is obtained (Fig. 9; Table 4) which is in support of the relative accuracy of our method.

5.1.2 Stable osmium isotope ratios by N-TIMS

For a single δ^{190}Os analysis by N-TIMS the internal precision (2 se; n ≤ 280 cycles, depending on 2 se outlier rejection) ranges between 0.010-0.040 ‰ when $^{188}OsO_3^-$ beam intensities vary from 6-0.43 V (~18 to 1 V ^{tot}Os beam; Fig. 7). These intensities were obtained for load sizes between 45 and 2.3 ng natural Os. Repeated analyses of double spiked reference solution DROsS, over approximately 22 months, yield an external reproducibility on δ^{190}Os of 0.029 ‰ (2 sd; *n* = 83; Fig. 8; Table 4). The majority of these analyses (*n* = 44) comprised a load of 10-20 ng natural Os, 20 analyses had a load of >20 ng, and 19 analyses were performed with less than 10 ng Os. That DROsS yields less precise and less reproducible results for N-TIMS than MC-ICP-MS is, predominantly, a consequence of the lower beam intensities at which the analyses were performed. Analyses of in-house pure Os solutions ROMIL, SpecPure and OsCaR show a similar precision and reproducibility (Fig. 7 and 9; Table 4). That ROMIL and SpecPure display a similar offset relative to DROsS for N-TIMS as for MC-ICP-MS analyses provides support to the accuracy of our method.

5.1.3 Radiogenic isotope ratios by MC-ICP-MS

The precision that can be obtained for $^{187}Os/^{188}Os$ and $^{186}Os/^{188}Os$ isotopic ratios is <100 ppm (2 se; n ≤ 280 cycles, depending on 2 se outlier rejection) when ^{187}Os and ^{186}Os average beam intensities are higher than ~0.06 V over the ~11 minutes of the analysis. When average beam intensities of >0.18 V are achieved this improves to ~40 ppm (Fig. 7). This is comparable with the precisions reported by Nowell et al. (2008; <40 ppm at high signal intensities)[36] and corresponds with the errors predicted by the model described in section 2.1 (30-40 ppm at 0.22 V; Fig. 7). Repeated analyses of double spiked reference standard DROsS yields a reproducibility of 123 and 138 ppm for $^{187}Os/^{188}Os$ and $^{186}Os/^{188}Os$, respectively (2 sd, *n* = 91). This is higher than that reported by Nowell et al. (2008)[36] for DROsS (19 ppm) but is comparable with the long-term reproducibilities reported for reference materials UMd (220 ppm for $^{187}Os/^{188}Os$ and 108 ppm for $^{186}Os/^{188}Os$) and DTM (149 ppm for $^{187}Os/^{188}Os$ and 67 ppm for $^{186}Os/^{188}Os$).

For radiogenic isotopic ratios we can use previous studies to assess the accuracy of our method. In addition, we have compared double spiked data with that from unspiked runs, and used DROsS for un-spiked sample-standard bracketing measurements. We have applied these methods to DROsS as well as to pure Os solutions ROMIL, SpecPure, and OsCaR. Taken together, the various samples encompass a significant range in $^{187}Os/^{188}Os$ isotopic ratios over which to test our analytical methods. Table 4 shows that all values obtained in this study, using the various methods, are within analytical uncertainty with one another as well as with previously published values of un-spiked DROsS measurements.[36, 37]

5.1.4 Radiogenic isotope ratios by N-TIMS

For N-TIMS analyses the internal precision on both $^{187}Os/^{188}Os$ and $^{186}Os/^{188}Os$ is <100 ppm (2 se; n ≤ 280 cycles, depending on 2 se outlier rejection) for analyses with average $^{187}OsO_3^-$ and $^{186}OsO_3^-$ beam intensities >0.03 V over the 280 cycles of analysis, and improves to <40 ppm at high signal intensities (>0.18 V; Fig. 7). This is slightly greater than the precisions reported by Luguet et al. (2008[37]; <30 ppm at >0.08 V). Repeated analyses of reference standard DROsS yield a reproducibility of 268 ppm and 361 ppm for $^{187}Os/^{188}Os$ and $^{186}Os/^{188}Os$ ratios, respectively (2 sd, *n* = 83) for loads varying between 2.3 and 45 ng natural Os. This is significantly higher than the values reported by Luguet et al. (2008[37]; 26 and 48 ppm, respectively). Where Luguet et al. (2008)[37] have only included analyses with $^{187}OsO_3^-$ and $^{186}OsO_3^-$ beam intensities of 80 mV or above we have taken analyses with intensities down to 20 mV into account. When excluding the analyses with beam intensities <80 mV on $^{187}OsO_3$- and $^{186}OsO_3$- we obtain a long-term reproducibility of 90 and 89 ppm, respectively (2 sd; *n* = 22). These slightly higher analytical uncertainties are related to error propagation inherent in double-spike deconvolution. That errors are higher than predicted by the model is, predominantly, because the error on the oxygen composition was not incorporated in the model, whereas it has been propagated for the actual analyses.

To assess the accuracy, we have compared the radiogenic values obtained by our DS method, with those determined for unspiked runs, and with previous studies (Table 4). All values are within analytical uncertainty of one another which demonstrates that our method is able to obtain accurate $^{187}Os/^{188}Os$ and $^{186}Os/^{188}Os$ isotopic ratios by N-TIMS. This provides a valuable quality control on the DS calculations and allows the acquisition of both the stable and radiogenic isotope composition within a single analytical run.

5.2. Geological materials

During the course of this study, we have measured four international geological reference materials. The selected materials cover a range of matrices; (1) UB-N[40], a serpentinised and fertile lherzolite from the Voges in France; (2) GP-13[41, 62], a fertile lherzolite from the Beni Bousera massif in Morocco; (3) CHR-Bkg [42, 43] and (4) CHR-Pt+[42, 63], which are both chromitites from the Shetland ophiolite in Scotland,

510 UK. Furthermore, we have analysed the ordinary H-chondrite Zag. Although this is not an international
511 reference material, sufficient sample material was available to perform several replicate analyses
512 allowing the exploration of another type of sample matrix. Stable and radiogenic Os isotope
513 compositions, together with Os abundances, are given in Table 5 and shown in Fig. 10-13.

514

515 ***5.2.1 Radiogenic osmium isotope compositions for geological materials***

516 We have shown that double spiked DROsS analyses display $^{187}Os/^{188}Os$ and $^{186}Os/^{188}Os$ ratios consistent
517 with previous published studies, and that ROMIL and SpecPure yield similar values for various methods
518 (i.e. non-DS, DS, standard sample bracketing). This means that although the main aim of this method is
519 to obtain high precision stable isotope data it also has the potential to provide radiogenic isotopic ratios
520 within the same analyses. This is particularly beneficial when dealing with limited amounts of available
521 sample material that only allows a single analysis. Furthermore, it significantly reduces processing and
522 measurement time.

523 Apart from three UB-N analyses, all data is obtained at average $^{187}OsO_3^-$ and $^{186}OsO_3^-$ beam
524 intensities of ≥0.01 V for N-TIMS ($^{total}Os \geq 1$ V) analyses and ^{187}Os and ^{186}Os ≥0.03 V for MC-ICP-MS
525 ($^{total}Os \geq 1$ V). The influence of the $^{17}O/^{16}O$ composition and OPZ on the accuracy of the isotopic
526 compositions is shown to be negligible at these intensities. Geological materials analysed in this study
527 display $^{187}Os/^{188}Os$ values that are consistent with the range of values obtained by previous studies (Fig.
528 10 and 13). However, a significant degree of irreproducibility (up to 7,400 ppm) can be observed which
529 will be discussed below. The variability observed for $^{186}Os/^{188}Os$ ratios is much smaller, 251-537 ppm,
530 and comparable with the long-term reproducibility obtained for N-TIMS DROsS analyses (361 ppm). The
531 $^{186}Os/^{188}Os$ ratios of all samples range from 0.119746 ± 42 to 0.119856 ± 47, which is in close
532 approximation of the upper mantle value (0.119837±5)[64] but consistently lower (Fig. 11). Assessment of
533 the accuracy of our $^{186}Os/^{188}Os$ values by direct comparison with previously published values for these
534 samples is not possible as they have not been measured for $^{186}Os/^{188}Os$ before. At this point, the reason
535 for the lower values is unclear and further investigation is required.

536

537 ***5.2.2 Stable osmium isotope compositions for geological materials***

538 The internal precision and external reproducibility on $\delta^{190}Os$ are similar to that obtained for pure Os
539 isotope solutions. One exception is the reproducibility reported by CHR-Pt+. This will be discussed in
540 more detail in the next section. Similar to Os standard solutions, replicate analyses of chondrite ZAG
541 show similar values for MC-ICP-MS and N-TIMS analyses, providing further support for the accuracy of
542 our method on a real sample matrix.

543 All reference materials are derived from Earth's mantle. The materials show no resolvable
544 variation at the 95 % c.i. level and provide an average $\delta^{190}Os$ value of 0.130 ± 0.032 ‰ (2 sd; *n* = 4). The

545 geological reference material CHR-Bkg displays the lightest composition of δ^{190}Os = 0.124 ± 0.020 ‰ (2
546 sd; *n* = 7) and chromitite CHR-Pt+ the heaviest at 0.162 ± 0.051 (2 sd; *n* = 4). Ordinary chondrite Zag
547 yields a δ^{190}Os value of +0.123 ± 0.018 ‰ (2 sd; *n* = 9) which is indistinguishable, within uncertainty,
548 from the mantle derived samples.

549 Interestingly, DROsS is the only material that displays a different, isotopically lighter,
550 composition relative to the other materials measured in this study. This offset could (a) be a product of
551 the chemical extraction of Os from the source material, or (b) reflect the original composition of the
552 material the Os was sourced from.

553

554 ***5.2.3 Effect of sample digestion***

555 In mantle rocks, osmium is concentrated in refractory accessory phases that are heterogeneously
556 distributed throughout the rock (the "nugget" effect). This has led to difficulties in repeating results
557 when considering Os abundances and ^{187}Os/^{188}Os ratios. Over the past two decades, various digestion
558 methods have been assessed in order to resolve this problem [e.g. 40, 44, 65, 66]. Acid attack digestions using
559 sealed glass Carius tubes (CT[23, 45]) and the high-pressure asher system (HPA[44]) are most frequently used.
560 This is because they are considered to be most efficient in attacking the highly resistant phases that are
561 likely to contain appreciable Os (such as Cr-spinel and platinum-group minerals). In this study, we have
562 applied both techniques to various geological materials. A limitation of both techniques is the maximum
563 amount of sample material that can be digested effectively (≤2 g). In the case of geological samples
564 with low Os abundances (e.g. most mantle material like UB-N, and nearly all crustal material) more than
565 2 g of material is needed to obtain high precision data. To circumvent this problem, we have digested
566 several sample aliquots of UB-N and GP-13, and combined them prior to solvent extraction. As for the
567 individual processed samples, each aliquot was spiked before digestion. As the proportion of spike is
568 one of the unknowns calculated during the resolution of the DS equation system, it should be noted
569 that reaching a 100 % yield across all aliquots during sample processing is not required to generate
570 accurate isotope ratios and concentration determinations, providing that spike-sample equilibration
571 occurs before loss of any Os during sample processing.

572 Apart from CHR-Pt+, replicate digestion of individual samples shows no detectable stable
573 isotope variation and no systematic difference between CT or HPA digestions. For the combined
574 aliquots of UB-N, relative to the single digestions, we do not observe any variation for stable Os isotopes
575 either (Fig. 12; Table 5). The two analyses of combined GP-13 aliquots show consistent stable isotope
576 compositions. By contrast, statistically resolvable variations in ^{187}Os/^{188}Os ratio and Os abundance were
577 observed in all the samples tested. In the case of UB-N and CHR-Bkg, ^{187}Os/^{188}Os is positively correlated
578 with 1/[Os] (Fig. 13). This co-variation was observed previously, in a more extensive study of UB-N, by
579 Meisel et al. (2003)[40]. The CHR-Bkg analyses reported within that study display a more limited variation
580 and no significant co-variation between Os abundance and radiogenic isotopic composition was

discussed. If we incorporate the CHR-Bkg data of Meisel et al. (2003)[40] they fall within the trend obtained in this study. The observed variation in radiogenic isotopes can be explained by incomplete digestion and/or sample heterogeneity. In both cases this indicates that within the digested material different phases, or phases of different generations, possess distinct radiogenic isotopic composition. The absence of stable Os isotope variation, for these particular aliquots, implies that there is no significant difference in stable isotope composition of the phases in these samples. As such, the type of digestion technique, or the combination of individual digestions, appears to have no influence on the stable isotope composition for these particular samples.

For CHR-Pt+ we observe a larger range in stable Os isotope compositions (δ^{190}Os = +0.129 – 0.198 ‰), which is reflected in the relatively poor reproducibility (0.051‰). The stable isotope data appear to co-vary with Os abundance, with the heavier values corresponding to higher Os abundance of 17.5 % (Fig. 12). As discussed before, variance in isotopic composition correlating with Os abundance may indicate that phases within the whole rock contain different stable isotopic signatures. Our preliminary data suggests that phases within chromitite CHR-Pt+ possess different stable Os isotopic compositions. Previous studies that focused on the origin of chromitites derived from the Cliff deposit in the Shetland Ophiolite concluded that initial PGE concentrations were caused by magmatic processes followed by a hydrothermal overprint which locally remobilized and re-concentrated the PGE.[67] This secondary process might be the source of Os stable isotope fractionation, but further investigation is required.

6. CONCLUSIONS

We have developed a method for high-precision measurement of stable Os isotope compositions by both plasma source (MC-ICP-MS) and thermal ionisation mass spectrometry (N-TIMS). The method utilizes a ^{188}Os-^{190}Os double spike that is added to the sample prior to digestion with a spike-sample proportion of 0.55:0.45. We show that the technique is robust when dealing with matrix effects and interference corrections on MC-ICP-MS, even for levels up to 10 % of the total Os concentration, and that the memory effect for MC-ICP-MS analyses is negligible. Analyses performed by N-TIMS show that the oxygen isotopic composition exerts a major control on the accuracy of the isotopic ratios. It is suggested that the oxygen isotopic composition is obtained for every specific run, by measuring the ^{18}O/^{16}O for each individual cycle, and calculating the ^{17}O/^{16}O ratio from the ^{18}O/^{16}O ratio, especially when the total Os signal intensity drops below 2 V.

The internal precision (2 se) on the δ^{190}Os measurement (permil difference of the ^{190}Os/^{188}Os ratio relative to reference standard DROsS) of a single analysis is 0.010-0.025 ‰ for MC-ICP-MS (~200 ng natural Os; *n* = 80 cycles) and 0.010-0.030 ‰ for N-TIMS (2.3-45 ng natural Os; *n* = 280 cycles). The long-term reproducibility of reference material DROsS is 0.016 ‰ (2 sd; *n* = 91) and 0.029 ‰ (2 sd; *n* = 83) for MC-ICP-MS and N-TIMS, respectively.

The method is shown to be capable of obtaining Os stable isotope compositions of terrestrial and extra-terrestrial materials with a high precision and reproducibility. The first data obtained for geological materials are all within analytical uncertainty of one another, despite the measurement of samples reflecting a range of source regions, chemical compositions, geological history, and radiogenic isotope ratios. Minor variations between different digestions of chromitite CHR-Pt+ hints at Os stable isotope fractionation as a result of Os remobilization due to hydrothermal alteration. Overall, our preliminary δ^{190}Os value for the Earth's upper mantle is +0.130 ± 0.032 ‰ (2 sd; *n* = 4), which is indistinguishable from a value of +0.123 ± 0.018 ‰ (2 sd; *n* = 9) obtained for the ordinary H-chondrite Zag.

Acknowledgements

We acknowledge financial support from an ERC starting Grant awarded to H. Williams (Habitable Planet 306655), which funded most of this analytical work, a Marie Curie COFUND International Junior Fellowship granted to M.-A. Millet, and a Durham University Scholarship awarded to J. Nanne. We thank C. Cloquet for providing us UB-N and A. Poirier for OsCaR. D. Selby, E. Dempsey, A. du Vivier, and A. Sproson are thanked for assistance in getting to grips with CT digestion and sample preparation, and C. Ottley for maintenance of the HPA.

FIGURE CAPTIONS

Figure 1 Results for an error (2 se) simulation on the stable isotope composition in ‰ amu^{-1} in case of a ^{188}Os-^{190}Os double spike. The red dot indicates that minimal error propagation of ~0.010 ‰ amu^{-1} (2 se) is obtained when using a 60 % ^{188}Os – 40 % ^{190}Os spike that is mixed with a sample in relative proportions of 55 % and 45 %. Note that errors are minimal (<0.020 ‰ amu^{-1}) over a large range of sample-spike mixtures (15 – 81 % sample fraction). The error model is based on the method of Millet and Dauphas (2014)[33] using the following parameters: 6 V; 80 x 8.3 sec integrations; 10^{11} Ω collectors; T= 290 K.

Figure 2 Results of double spiked DROsS analyses measured using MC-ICP-MS (closed symbols) at variable beam intensities to assess the effect of beam intensity and the on-peak zero on the accuracy of the $\delta^{190}Os$ and $^{187}Os/^{188}Os$ composition. Data show that all measurements display $\delta^{190/188}Os$ and $^{187}Os/^{188}Os$ compositions within analytical uncertainty of the long-term reproducibility as determined for >10 V analyses. The black dotted line indicates the average DROsS value, as obtained from the >10 V analyses, with the ±2 sd represented by the grey band.

Figure 3 Results of doping tests to assess the robustness of the method against residual matrix effects on the MC-ICP-MS. Data show that all measurements display $\delta^{190/188}Os$ compositions within analytical uncertainty of undoped DROsS analyses for residual element abundances up to 10 % of the total Os concentration. The percentages indicate the presence of each named element at x% of the Os abundance, e.g. Si was present at 5% of the Os abundance. The black dotted line indicates the average DROsS value with the ±2 sd represented by the grey shaded band as obtained in this study. Lith = lithophile elements (Si, Al, Mg, Fe, Ca, Ti, Ni, and Cr); PGE = Platinum Group Elements (Ru, Rh, Pd, Ir, and Pt).

Figure 4 The difference in measured $^{18}O/^{16}O$ ratios between the first and the last 20 cycles of double spiked DROsS analyses (green circles) show an average variability of -1.1 ‰ (green dotted line). For clarity, two values with a deviation of -12 ‰, at 1.4 V and 1.7 V, are excluded. The variability is shown to increase with decreasing beam intensity and seems to be larger when samples are run twice for 280 cycles. Open symbols represent analyses where the oxygen composition has been measured before and after the main run.

Figure 5 Residual correlation for double spiked DROsS analyses by N-TIMS between the measured $^{17}O/^{16}O$ (grey circles) and Os isotopic compositions; (a) $\delta^{190/188}Os$, (b) $^{187}Os/^{188}Os$, and (c) $^{186}Os/^{188}Os$. No residual correlation is observed when the $^{17}O/^{16}O$ is calculated from the measured $^{18}O/^{16}O$ ratio (green circles). The offset from the expected DROsS value is seen to increase with decreasing beam intensities (d-f), with a reduced offset when using calculated $^{17}O/^{16}O$ ratios. With decreasing signal intensity, (d) $\delta^{190/188}Os$ values seem to slightly drift towards heavier values, and (e) $^{187}Os/^{188}Os$ and (f) $^{186}Os/^{188}Os$ towards lower values. The black dashed line represents the expected DROsS value.

Figure 6 Measured $^{18}O/^{16}O$ vs. $^{17}O/^{16}O$ ratios for DROsS analyses run at a total Os beam intensity of >2 V closely follow the Terrestrial Fractionation Line (TFL). Analyses are divided based on the beam intensity on mass 242 (<5 mV; 5-10 mV; >10 mV). The TFL was calculated using a slope of 0.526 which translates to an roughly linear slope of 0.0994 x + 0.000183, where x is $^{18}O/^{16}O$, over a $^{18}O/^{16}O$ interval of 0.002007 to 0.002055, the range in $^{18}O/^{16}O$ obtained in this study. Also shown are oxygen isotope ratios from N-TIMS measurements in previous studies: Nagai and Yokoyama (2016)[51]; Worsham et al. (2016) [52]; Luguet et al. (2008)[37]; Griselin et al. (2001)[68]; Chavagnac (1998)[69]; Thirlwall (1991)[70]; Reisberg and Zindler (1986)[71]; Nyquist in Wasserburg et al. (1981); Wasserburg et al. (1981)[72]; Nier (1950)[73].

Figure 7 The analytical precision (2 se) on (a) $\delta^{190/188}Os$ and (b) $^{187}Os/^{188}Os$ plotted against the average (a) $^{188}OsO_3^-$ and (b) $^{187}OsO_3^-$ beam intensity (V) for analyses of reference material DROsS, and other pure Os solutions by MC-ICP-MS or N-TIMS. The dashed (MC-ICP-MS) and dotted (N-TIMS) lines in (a) indicate the modelled error calculated using the method of Millet and Dauphas (2014)[33] using the following parameters: 80 x 8.3 seconds integrations for MC-ICP-MS and 280 x 8.3 seconds for N-TIMS; 10^{11} Ω collectors; T= 290 K. Note that the lower theoretical error for N-TIMS results from the larger amount of cycles incorporated.

Figure 8 Repeated analyses of reference material DROsS on both MC-ICP-MS (squares) and N-TIMS (circles) obtained during multiple analytical sessions over a time period of 22 months. Analyses have been organized on beam intensity, note that N-TIMS analyses are obtained at lower beam intensities. Sample size is approximately

200 ng natural Os for MC-ICP-MS and ranges between 2.3 and 45 ng natural Os for N-TIMS measurements, with ^{total}Os beam intensities of >4 V for MC-ICP-MS analyses and >1 V for analyses by N-TIMS. Error bars quote the 2 se error on the individual analysis, the grey band represents the ±2 sd of all analyses. Symbols in yellow correspond to the annotated beam intensity.

Figure 9 The $\delta^{190/188}$Os value obtained for repeat analyses of pure Os solutions ROMIL (triangle), SpecPure (circle) and OsCaR (diamond) by both MC-ICP-MS (closed symbols) and N-TIMS (open symbols) obtained during the course of this study. The striped, filled symbols indicate sample-standard bracketing data. All Os solutions show a similar reproducibility as obtained for reference standard DROsS. Values obtained for ROMIL and SpecPure on MC-ICP-MS and N-TIMS show values within analytical uncertainty supporting the accuracy of our method. The grey bands indicate the reproducibility (±2 sd) obtained by MC-ICP-MS and N-TIMS. Error bars represent the 2 se error of an individual analysis.

Figure 10 The ^{187}Os/^{188}Os isotope ratios of geological materials UB-N, GP-13, CHR-Bkg, CHR-Pt+ and Zag analysed by MC-ICP-MS (closed symbols) or N-TIMS (open symbols) display values consistent with previous studies (grey bars). Literature data for maximum and minimum values: UB-N – ref. 40, 74; GP-13 – ref. 75, 76; CHR-Bkg – ref 40; CHR-Pt+ - no previous published data; Zag – ref 3, 4.

Figure 11 The ^{186}Os/^{188}Os ratios of geological materials UB-N, GP-13, CHR-Bkg, CHR-Pt+ and Zag analysed by MC-ICP-MS (closed symbols) or N-TIMS (open symbols). Most samples plot below the upper mantle value of 0.119837±5 (2 sd; Ireland et al., 2011[64]). CT = Carius tube digestions, all other sample aliquots are processed using the high-pressure asher system. * = an analysis for which digestions were combined prior to chemical Os extraction. Error bars indicate the 2 se on the individual analysis.

Figure 12 Osmium stable isotope compositions ($\delta^{190/188}$Os) of geological materials UB-N, GP-13, CHR-Bkg, CHR-Pt+ and Zag analysed by MC-ICP-MS (closed symbols) or N-TIMS (open symbols). Symbols are ordered from high to low Os concentration. Apart from Zag, which is an ordinary chondrite, all samples are reference materials sourced by the Earth's mantle. Symbols as in Fig. 11.

Figure 13 Correlation between ^{187}Os/^{188}Os ratio and 1/[Os] for reference materials UB-N (circles) and CHR-Bkg (triangles), as obtained for independently processed sample aliquots in this study (open symbols). Included are data as obtained by Meisel et al. (2003[40]; filled symbols).

TABLE CAPTIONS

Table 1 Osmium isotopic ratios of reference standard DROsS, as determined by Nowell et al. (2008)[36] normalized to $^{189}Os/^{188}Os$ to correct for mass bias, and of the ^{188}Os-^{190}Os double spike (DS) as used in this study. The quoted error on DROsS represents the 2 sd on 21 analyses, and the error on the DS is the relative 2 se on the analysis used to obtain the DS composition.

Table 2 Faraday cup configuration used for osmium isotope measurements by static multi-collection on a Thermo Neptune MC-ICP-MS and Thermo Triton Plus N-TIMS at Durham University. Only principal ions measured are listed, see ref. 37 (Luguet et al., 2008) for a full list of known polyatomic interferences.

Table 3 Osmium stable isotope compositions ($\delta^{190/188}Os$) of analytical tests on the MC-ICP-MS showing the robustness of our methodology with regards to (i) signal intensity and (ii) matrix effects and interference corrections. The percentages indicate the presence of each named element at x% of the Os abundance, e.g. Si was present at 5 % of the Os abundance. *Lith = Lithophile elements (Si, Al, Mg, Fe, Ca, Ti, Ni, and Cr); **PGE = Platinum Group Elements (Ru, Rh, Pd, Ir, and Pt).

Table 4 Average osmium stable and radiogenic isotope ratios of DROsS, SpecPure, ROMIL and OsCaR obtained in this study using: the double spike (DS) method; sample-standard bracketing by MC-ICP-MS, using non DS solutions and DROsS as the reference bracketing standard; and un-spiked runs by N-TIMS. For comparison the radiogenic isotope composition of DROsS as obtained by previous studies is included (Nowell et al., 2008[36]; Luguet et al., 2008[37]). Note that the better reproducibility (2 sd) for MC-ICP-MS relative to N-TIMS is, predominantly, related to difference in beam intensities at which analyses have been made (11-18 V vs. 1-18 V total Os beam, respectively). * - Four individual sample-standard bracketing sessions were run, on different days, and include 16 analyses all together. Presented are the average and 2 sd on the averages of the four analytical sessions.

Table 5 Osmium stable ($\delta^{190/188}Os$) and radiogenic ($^{187}Os/^{188}Os$ and $^{186}Os/^{188}Os$) isotope compositions, and Os abundances of geological materials obtained by either MC-ICP-MS or N-TIMS. Samples are digested using carius tubes (CT) or the high-pressure asher (HPA) system. W. mean = weighted mean; * = aliquots of sample material that are combined after digestion and prior to chemical separation of Os.

740 **FIGURES**

741 **Figure 1**

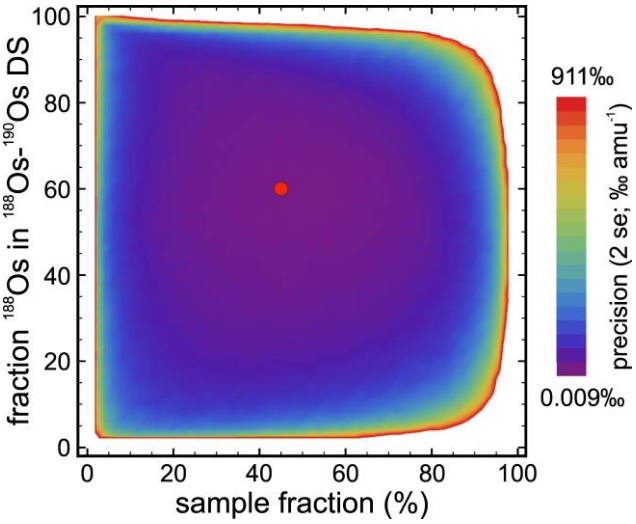

742

743 **Figure 2**

744

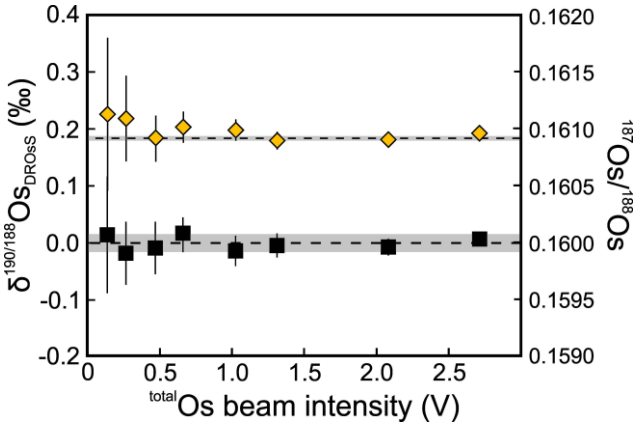

745 **Figure 3**

746

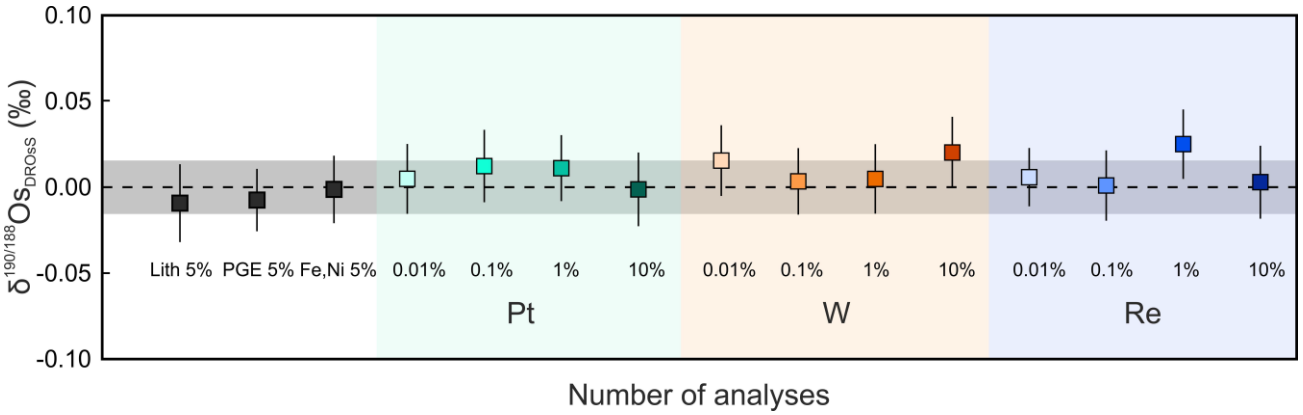

747 **Figure 4**

748

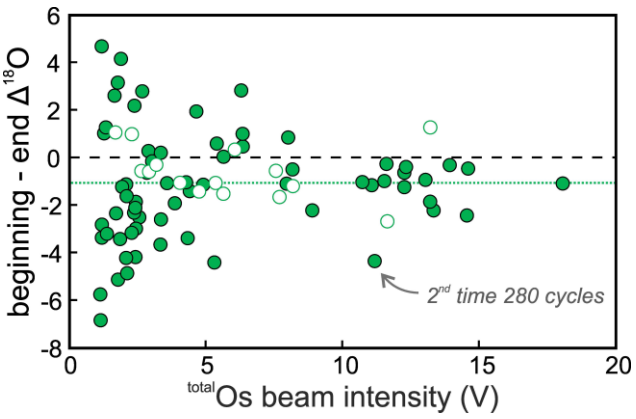

749 **Figure 5**

750

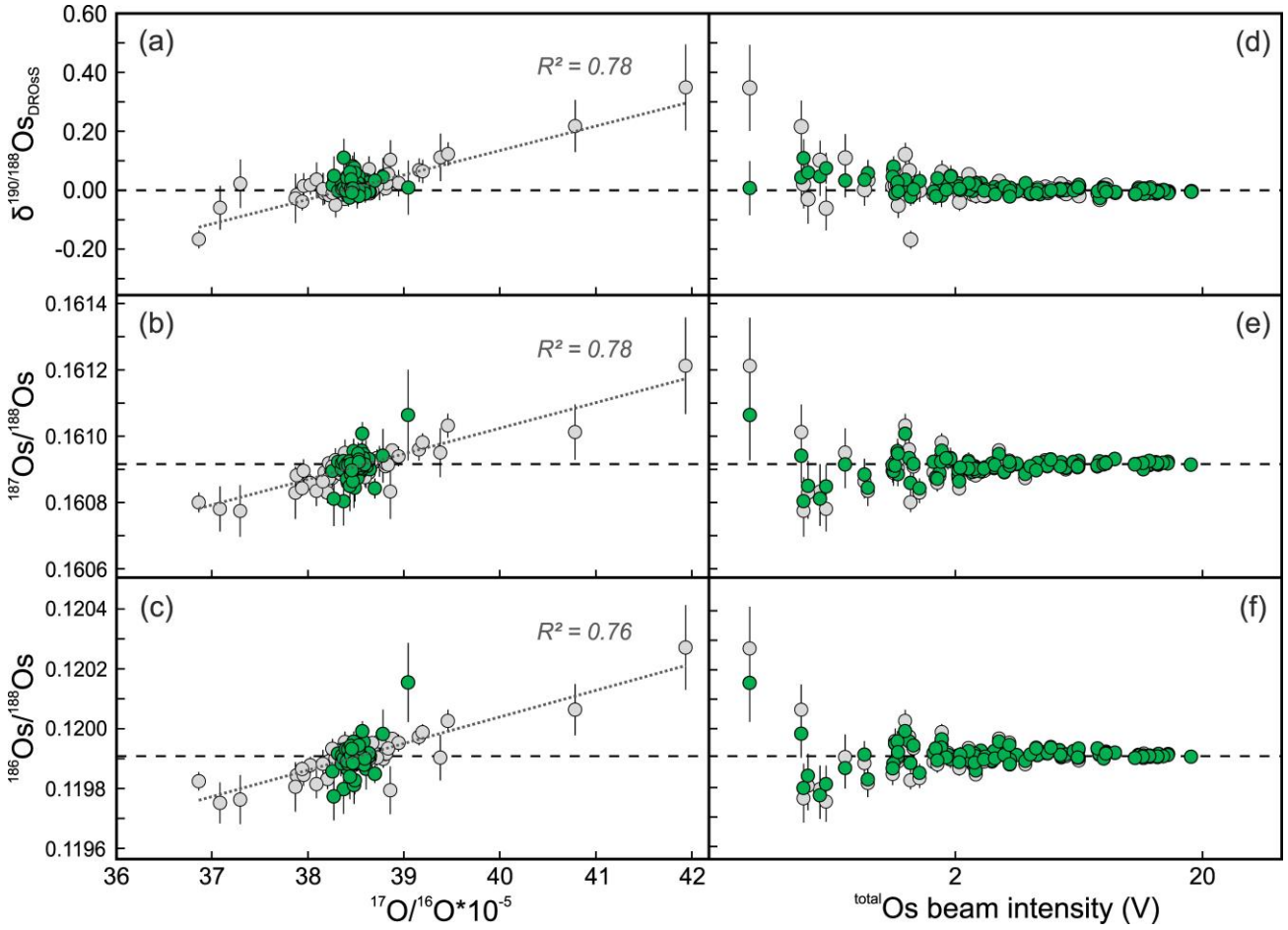

751 **Figure 6**

752

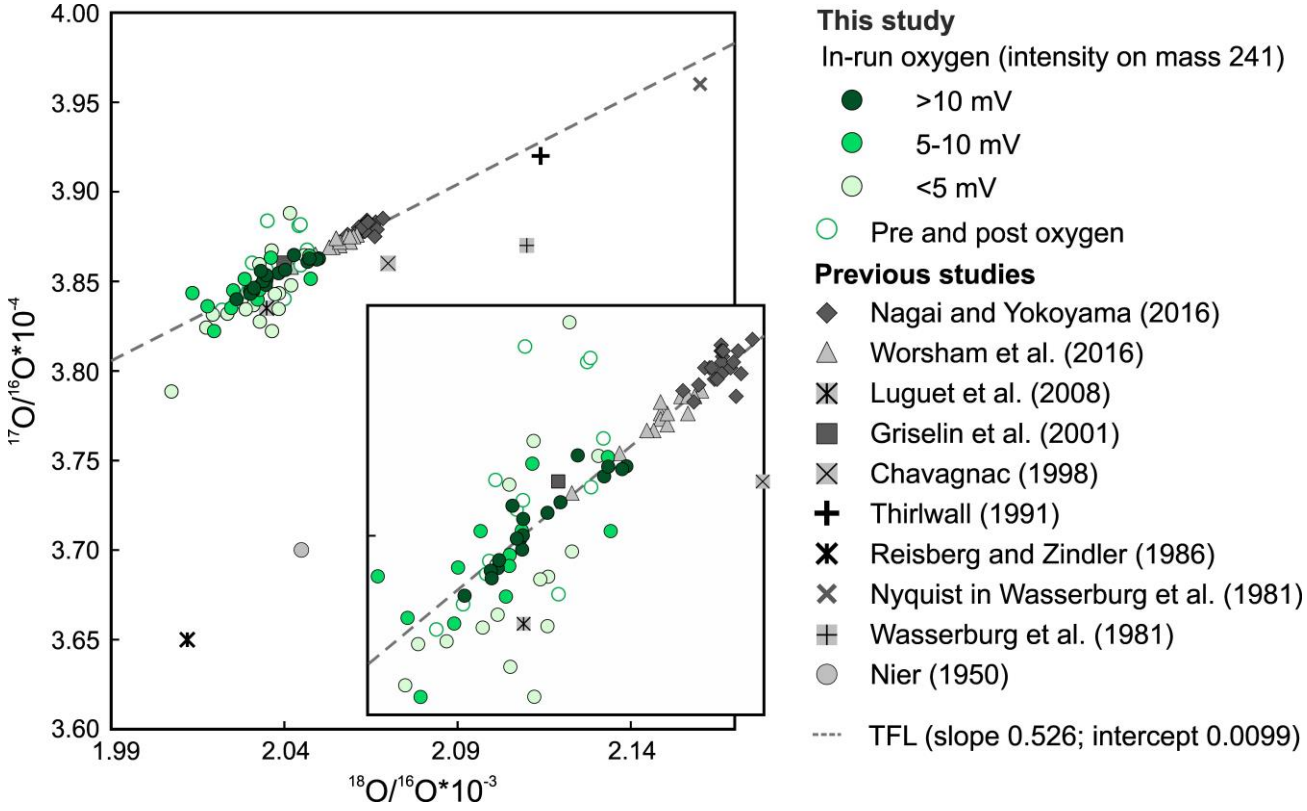

753 **Figure 7**

754

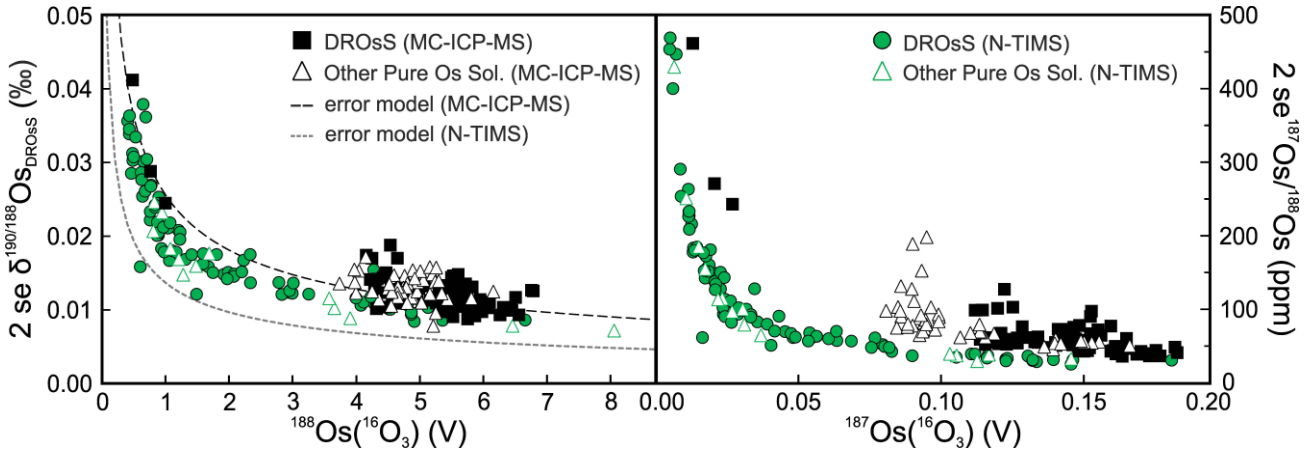

Figure 8

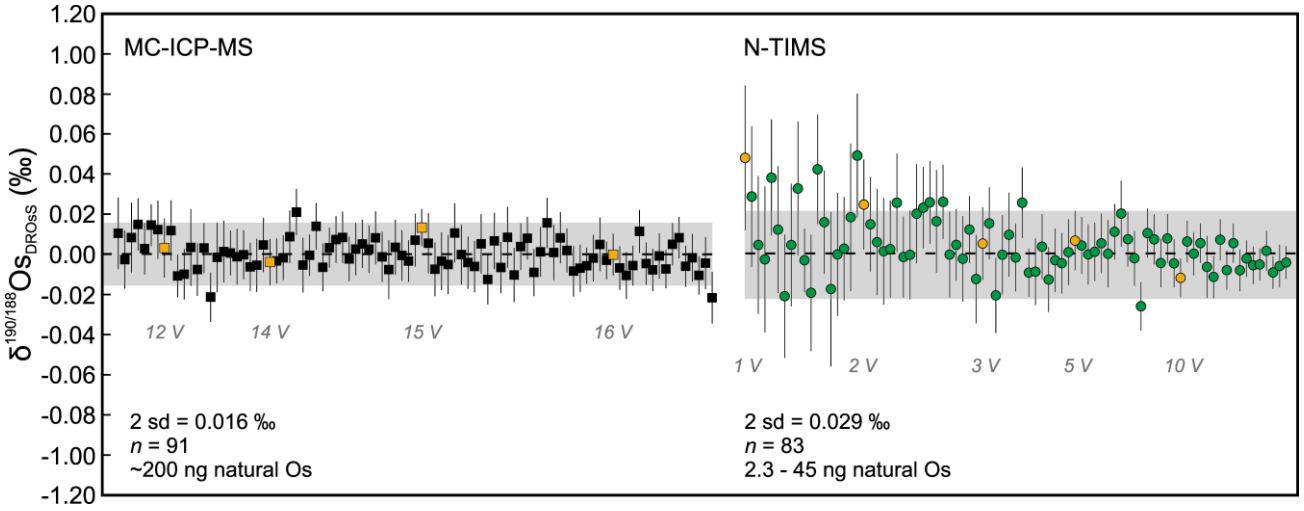
MC-ICP-MS
N-TIMS
$\delta^{190/188}Os_{DROsS}$ (‰)
1.20
1.00
0.08
0.06
0.04
0.02
0.00
-0.02
-0.04
-0.06
-0.08
-1.00
-1.20
12 V
14 V
15 V
16 V
1 V
2 V
3 V
5 V
10 V
2 sd = 0.016 ‰
n = 91
~200 ng natural Os
2 sd = 0.029 ‰
n = 83
2.3 - 45 ng natural Os

757 **Figure 9**

758

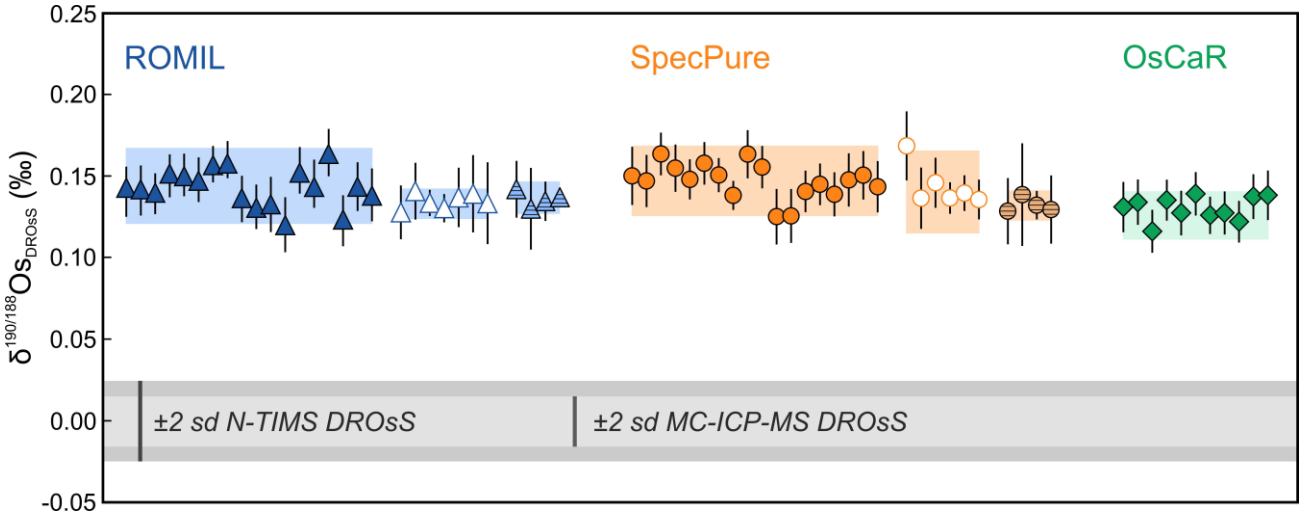

759 **Figure 10**

760

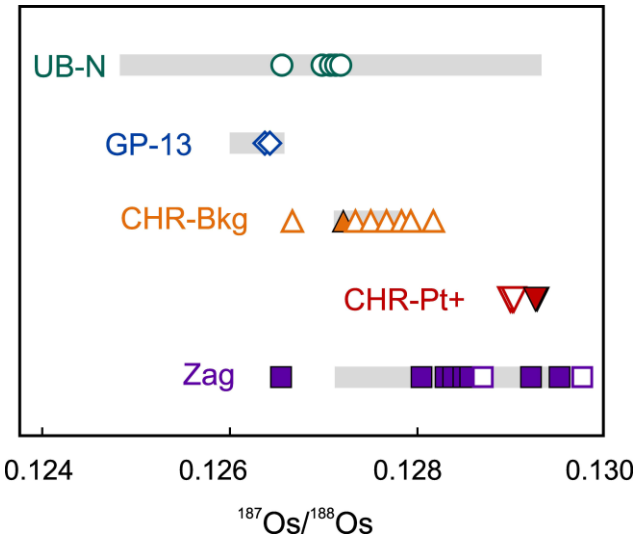

761 **Figure 11**

762

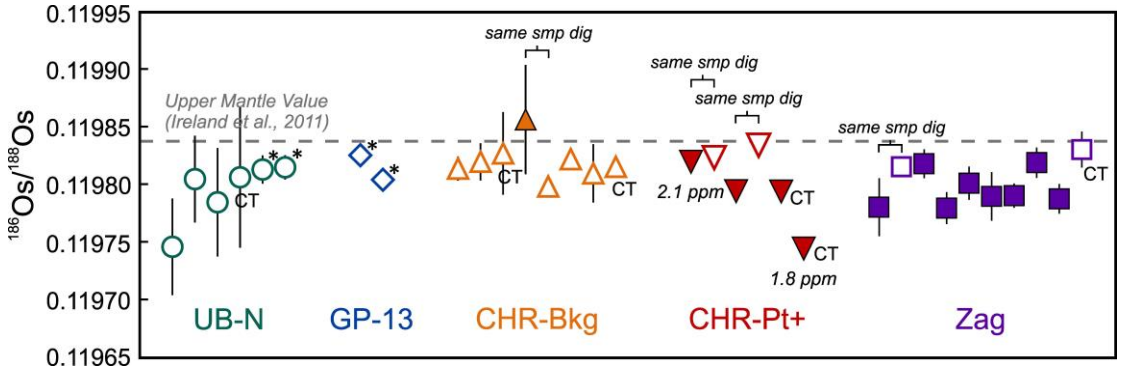

763 **Figure 12**

764

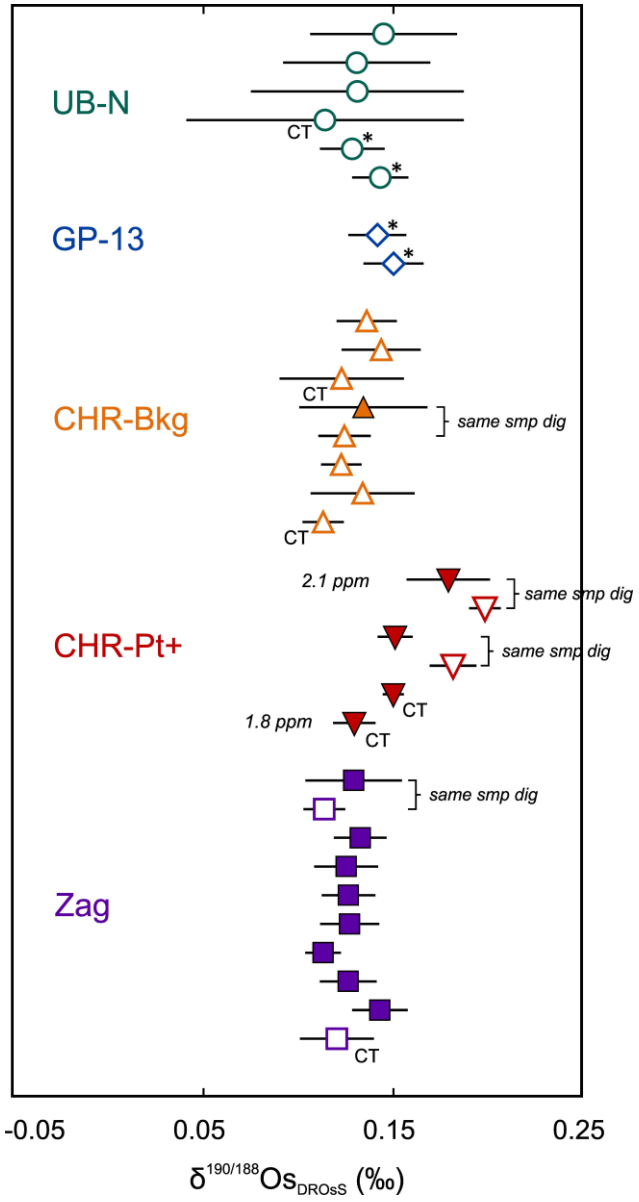

765 **Figure 13**

766

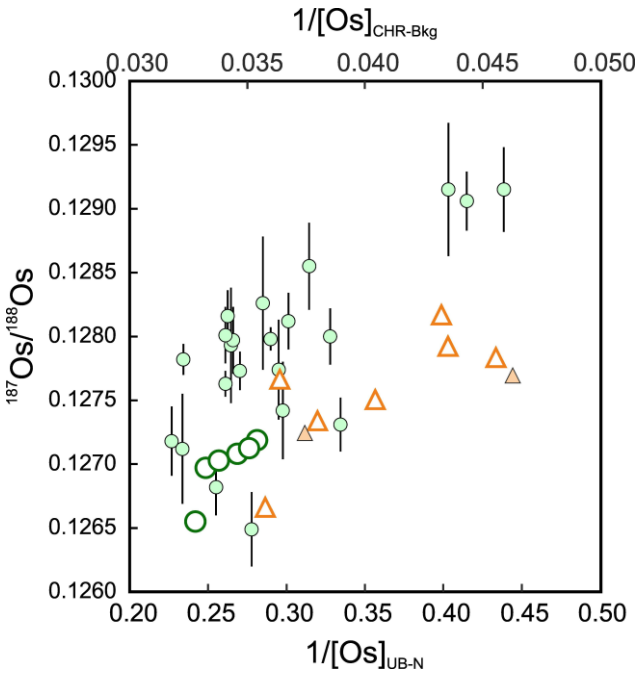

TABLES

Table 1

	$^{186}Os/^{188}Os$	$^{187}Os/^{188}Os$	$^{189}Os/^{188}Os$	$^{190}Os/^{188}Os$	$^{192}Os/^{188}Os$
Reference std DROsS (±2 sd)	0.119909 ± 04	0.160916 ± 04	1.219780	1.983979 ± 30	3.083580 ± 14
^{188}Os - ^{190}Os spike (±2 se)	0.001372 ± 54	0.001239 ± 58	0.020944 ± 11	0.684512 ± 06	0.036517 ± 14

771 **Table 2**

Cup	L4	L3	L2	L1	Ax	H1	H2	H3	H4
MC-ICP-MS									
Analyte isotopes	^{183}W	^{185}Re	^{186}Os	^{187}Os	^{188}Os	^{189}Os	^{190}Os	^{192}Os	^{194}Pt
N-TIMS									
Mass		*232*	*234*	*235*	*236*	*237*	*238*	*240*	
Seq1		$^{184}Os^{16}O_3^-$	$^{186}Os^{16}O_3^-$	$^{187}Os^{16}O_3^-$	$^{188}Os^{16}O_3^-$	$^{189}Os^{16}O_3^-$	$^{190}Os^{16}O_3^-$	$^{192}Os^{16}O_3^-$	
Mass		*236*	*238*	*239*	*240*	*241*	*242*		
Seq2		$^{188}Os^{16}O_3^-$	$^{190}Os^{16}O_3^-$		$^{192}Os^{16}O_3^-$	$^{192}Os^{16}O_2{}^{17}O^-$	$^{192}Os^{16}O_2{}^{18}O^-$		

772

773 **Table 3**

(i) Signal intensity			
Concentration	**δ^{190}Os**	**2 se**	**^{Total}Os (V)**
0.10 ppm	0.007	0.012	2.71
0.08 ppm	-0.007	0.014	2.08
0.05 ppm	-0.004	0.021	1.31
0.04ppm	-0.014	0.026	1.02
0.03 ppm	0.017	0.033	0.66
0.02 ppm	-0.009	0.045	0.47
0.01 ppm	-0.018	0.055	0.26
0.005 ppm	0.014	0.102	0.14
(ii) Matrix effects and interference corrections			
Doping element	**δ^{190}Os**	**2 se**	
Lith* 5%	-0.009	0.018	
PGE** 5%	-0.008	0.014	
Fe, Ni 5%	-0.001	0.017	
Pt 0.01%	0.005	0.017	
Pt 0.1%	0.012	0.018	
Pt 1%	0.011	0.016	
Pt 10%	-0.001	0.017	
W 0.01%	0.016	0.017	
W 0.1%	0.003	0.015	
W 1%	0.005	0.017	
W 10%	0.020	0.016	
Re 0.01%	0.006	0.012	
Re 0.1%	0.001	0.013	
Re 1%	0.025	0.014	
Re 10%	0.003	0.017	

774

775 **Table 4**

	n	δ^{190}Os	2 sd	^{187}Os/^{188}Os	2 sd	^{186}Os/^{188}Os	2 sd
DROsS							
DS MC-ICP-MS	*91*	0.000	0.016	0.160916	0.000020	0.119909	0.000017
DS N-TIMS	*83*	0.001	0.029	0.160916	0.000043	0.119909	0.000043
un-spiked	*14*	-	-	0.160919	0.000031	-	-
previous study (MC-ICP-MS; Nowell et al., 2008[35])	*21*	-	-	0.160924	0.000003	0.119920	0.000002
previous study (N-TIMS; Luguet et al. ,2008[36])	*8*	-	-	0.160924	0.000004	0.119932	0.000006
ROMIL							
DS MC-ICP-MS	*18*	0.144	0.023	0.106827	0.000047	0.119806	0.000017
DS N-TIMS	*7*	0.133	0.009	0.106857	0.000042	0.119803	0.000023
sample-std bracketing MC-ICP-MS	*4**	0.137	0.010	0.106861	0.000024	0.119806	0.000007
un-spiked	*3*	-	-	0.106878	0.000032	-	-
SpecPure							
DS MC-ICP-MS	*18*	0.147	0.022	0.149162	0.000026	0.119890	0.000019
DS N-TIMS	*6*	0.140	0.025	0.149161	0.000053	0.119889	0.000031
sample-std bracketing MC-ICP-MS	*4**	0.132	0.009	0.149163	0.000012	0.119885	0.000016
un-spiked	*3*	-	-	0.149180	0.000088	-	-
OsCaR							
DS MC-ICP-MS	*11*	0.126	0.015	0.128298	0.000022	0.119816	0.000014

776

777 **Table 5**

				smp weight (g)	$^{total}Os$ (V)	$^{188}Os(O_3^-)$	^{187}Os (O_3^-)	$\delta^{190}Os$	2 se	$^{187}Os/^{188}Os$	2 se	$^{186}Os/^{188}Os$	2 se	[Os] ng g^{-1}	2 se
UB-N	1	HPA	N-TIMS	2.51	0.98	0.37	0.008	0.145	0.039	0.126555	0.000040	0.119746	0.000042	4.13	0.002
	2	HPA	N-TIMS	2.51	1.16	0.43	0.009	0.131	0.039	0.126983	0.000039	0.119804	0.000037	4.02	0.002
	3	HPA	N-TIMS	2.49	0.92	0.35	0.007	0.131	0.056	0.127061	0.000047	0.119784	0.000047	3.89	0.003
	4	CT	N-TIMS	2.49	0.82	0.33	0.006	0.114	0.073	0.127073	0.000057	0.119806	0.000061	3.72	0.002
	5*	HPA	N-TIMS	6.03	3.99	1.53	0.030	0.128	0.017	0.127128	0.000011	0.119813	0.000012	3.62	0.001
	6*	HPA	N-TIMS	5.99	3.09	1.19	0.023	0.143	0.015	0.127181	0.000011	0.119815	0.000010	3.55	0.001
w. mean								**0.136**		**0.127126**		**0.119813**		**3.64**	
2 sd								**0.022**		**0.000453**		**0.000053**		**0.46**	
GP-13	1*	HPA	N-TIMS	4.02	4.95	1.87	0.039	0.142	0.015	0.126372	0.000010	0.119825	0.000010	3.87	0.002
	2*	HPA	N-TIMS	4.05	4.67	1.76	0.036	0.150	0.016	0.126426	0.000009	0.119804	0.000009	3.82	0.002
w. mean								**0.146**		**0.126401**		**0.119813**		**3.84**	
2 sd								**0.012**		**0.000077**		**0.000030**		**0.07**	
CHR-Bkg	1	HPA	N-TIMS	0.93	4.68	1.75	0.037	0.136	0.016	0.126667	0.000010	0.119813	0.000010	27.96	0.01
	2	HPA	N-TIMS	0.92	2.74	1.03	0.022	0.144	0.021	0.127671	0.000016	0.119819	0.000016	27.48	0.01
	3	CT	N-TIMS	0.55	1.21	0.46	0.009	0.123	0.033	0.127340	0.000034	0.119827	0.000035	26.32	0.01
	4a	HPA	MC-ICP-MS	2.06	3.42	1.29	0.026	0.134	0.034	0.127210	0.000040	0.119856	0.000047	24.72	0.001
	4b	HPA	N-TIMS	"	6.02	2.30	0.046	0.124	0.014	0.127503	0.000008	0.119798	0.000009	24.72	0.001
	5	HPA	N-TIMS	0.92	9.64	3.80	0.070	0.123	0.011	0.128170	0.000006	0.119822	0.000006	23.11	0.01
	6	CT	N-TIMS	0.58	1.81	0.71	0.013	0.134	0.027	0.127929	0.000025	0.119809	0.000025	22.97	0.01
	7	HPA	N-TIMS	0.92	9.50	3.79	0.067	0.113	0.011	0.127830	0.000006	0.119815	0.000007	21.95	0.01
w. mean								**0.124**		**0.127803**		**0.119818**		**24.73**	
2 sd								**0.020**		**0.000945**		**0.000034**		**4.39**	
CHR-Pt+	1a	HPA	MC-ICP-MS	0.23	15.54	5.62	0.129	0.179	0.022	0.128992	0.000011	0.119819	0.000009	2121	6
	1b	HPA	N-TIMS	"	15.35	5.59	0.129	0.198	0.008	0.129278	0.000004	0.119823	0.000005	2121	4
	2a	HPA	MC-ICP-MS	0.25	25.05	9.41	0.195	0.151	0.009	0.129012	0.000006	0.119794	0.000004	1805	6
	2b	HPA	N-TIMS	"	6.60	2.49	0.052	0.181	0.012	0.129260	0.000008	0.119833	0.000008	1805	6

	3	CT	MC-ICP-MS	0.25	23.15	8.76	0.178	0.150	0.005	0.129029	0.000004	0.119796	0.000003	1785	4
	4	CT	MC-ICP-MS	0.25	12.02	4.54	0.092	0.129	0.011	0.128993	0.000012	0.119744	0.000009	1747	6
w. mean								**0.162**		**0.129033**		**0.119804**		**1879**	
2 sd								**0.051**		**0.000273**		**0.000064**		**349**	
ZAG	1a	HPA	MC-ICP-MS	0.24	6.73	2.51	0.049	0.129	0.025	0.129518	0.000018	0.119780	0.000025	929	6
	1b	HPA	N-TIMS	""	3.28	1.26	0.025	0.114	0.011	0.129759	0.000007	0.119815	0.000007	929	4
	2	HPA	MC-ICP-MS	0.25	8.94	3.28	0.067	0.133	0.014	0.126549	0.000011	0.119818	0.000012	926	6
	3	HPA	MC-ICP-MS	0.25	9.16	3.38	0.068	0.125	0.017	0.128046	0.000014	0.119779	0.000013	905	6
	4	HPA	MC-ICP-MS	0.25	8.63	3.18	0.064	0.126	0.014	0.128557	0.000012	0.119801	0.000014	904	6
	5	HPA	MC-ICP-MS	0.50	5.78	2.15	0.042	0.127	0.016	0.129214	0.000028	0.119789	0.000021	892	3
	6	HPA	MC-ICP-MS	0.50	12.05	4.47	0.088	0.113	0.009	0.128650	0.000011	0.119790	0.000010	887	3
	7	HPA	MC-ICP-MS	0.25	8.73	3.24	0.064	0.126	0.015	0.128382	0.000013	0.119819	0.000013	884	6
	8	HPA	MC-ICP-MS	0.25	9.03	3.40	0.065	0.143	0.015	0.128303	0.000014	0.119787	0.000013	861	6
	9	CT	N-TIMS	0.08	5.05	1.90	0.040	0.120	0.019	0.128699	0.000015	0.119830	0.000015	839	17
w. mean								**0.123**		**0.128407**		**0.119804**		**896**	
2 sd								**0.018**		**0.001791**		**0.000036**		**59**	

778

REFERENCES

1. S. B. Shirey and R. J. Walker, *Annual Review of Earth and Planetary Sciences*, 1998, **26**, 423-500.
2. R. W. Carlson, *Lithos*, 2005, **82**, 249-272.
3. R. J. Walker, M. F. Horan, J. W. Morgan, H. Becker, J. N. Grossman and A. E. Rubin, *Geochimica et Cosmochimica Acta*, 2002, **66**, 4187-4201.
4. T. Meisel, R. J. Walker and J. W. Morgan, *Nature*, 1996, **383**, 517-520.
5. A. D. Brandon, R. J. Walker, J. W. Morgan, M. D. Norman and H. M. Prichard, *Science*, 1998, **280**, 1570-1573.
6. R. J. Walker, *Chemie der Erde-Geochemistry*, 2009, **69**, 101-125.
7. J. E. Snow and L. Reisberg, *Earth and Planetary Science Letters*, 1995, **133**, 411-421.
8. A. Meibom, N. H. Sleep, C. P. Chamberlain, R. G. Coleman, R. Frei, M. T. Hren and J. L. Wooden, *Nature*, 2002, **419**, 705-708.
9. A. D. Brandon, R. A. Creaser, S. B. Shirey and R. W. Carlson, *Science*, 1996, **272**, 861-863.
10. D. G. Pearson, S. W. Parman and G. M. Nowell, *Nature*, 2007, **449**, 202-205.
11. C. W. Dale, A. Gannoun, K. W. Burton, T. W. Argles and I. J. Parkinson, *Earth and Planetary Science Letters*, 2007, **253**, 211-225.
12. H. J. Stein, K. Sundblad, R. J. Markey, J. W. Morgan and G. Motuza, *Mineralium Deposita*, 1998, **33**, 329-345.
13. K. W. Burton, *Journal of Geochemical Exploration*, 2006, **88**, 262-265.
14. W. J. Pegram, S. Krishnaswami, G. E. Ravizza and K. K. Turekian, *Earth and Planetary Science Letters*, 1992, **113**, 569-576.
15. B. Peucker-Ehrenbrink and G. Ravizza, *Terra Nova*, 2000, **12**, 205-219.
16. S. G. Nielsen, M. Rehkämper and A. N. Halliday, *Geochimica et Cosmochimica Acta*, 2006, **70**, 2643-2657.
17. G. A. Brennecka, L. E. Borg, I. D. Hutcheon, M. A. Sharp and A. D. Anbar, *Earth and Planetary Science Letters*, 2010, **291**, 228-233.
18. J. B. Creech, J. A. Baker, M. R. Handler, M. Schiller and M. Bizzarro, *Journal of Analytical Atomic Spectrometry*, 2013, **28**, 853-865.
19. J. B. Creech, J. A. Baker, M. R. Handler and M. Bizzarro, *Chemical Geology*, 2014, **363**, 293-300.
20. C. H. Stirling, M. B. Andersen, E.-K. Potter and A. N. Halliday, *Earth and Planetary Science Letters*, 2007, **264**, 208-225.
21. M. Rehkämper, M. Frank, J. R. Hein, D. Porcelli, A. Halliday, J. Ingri and V. Liebetrau, *Earth and Planetary Science Letters*, 2002, **197**, 65-81.
22. S. G. Nielsen, M. Rehkamper, M. D. Norman, A. N. Halliday and D. Harrison, *Nature*, 2006, **439**, 314-317.
23. J. J. Shen, D. A. Papanastassiou and G. J. Wasserburg, *Geochimica et Cosmochimica Acta*, 1996, **60**, 2887-2900.
24. J. L. Birck, M. R. Barman and F. Capmas, *Geostandards Newsletter*, 1997, **21**, 19-27.
25. M. H. Dodson, *Journal of Scientific Instruments*, 1963, **40**, 289-295.
26. S. J. G. Galer, *Chemical Geology*, 1999, **157**, 255-274.
27. M.-A. Millet, J. A. Baker and C. E. Payne, *Chemical Geology*, 2012, **304**, 18-25.
28. A. D. Brandon, M. Humayun, I. S. Puchtel, I. Leya and M. Zolensky, *Science*, 2005, **309**, 1233-1236.
29. T. Yokoyama, V. K. Rai, C. M. D. Alexander, R. S. Lewis, R. W. Carlson, S. B. Shirey, M. H. Thiemens and R. J. Walker, *Earth and Planetary Science Letters*, 2007, **259**, 567-580.
30. T. Yokoyama, C. M. D. Alexander and R. J. Walker, *Earth and Planetary Science Letters*, 2010, **291**, 48-59.
31. N. Wittig, M. Humayun, A. D. Brandon, S. Huang and I. Leya, *Earth and Planetary Science Letters*, 2013, **361**, 152-161.
32. C. Siebert, T. F. Nägler and J. D. Kramers, *Geochemistry, Geophysics, Geosystems*, 2001, **2**, 1032.
33. M.-A. Millet and N. Dauphas, *Journal of Analytical Atomic Spectrometry*, 2014, **29**, 1444-1458.
34. M.-A. Millet, N. Dauphas, N. D. Greber, K. W. Burton, C. W. Dale, B. Debret, C. G. Macpherson, G. M. Nowell and H. M. Williams, *Earth and Planetary Science Letters*, 2016, **449**, 197-205.
35. J. F. Rudge, B. C. Reynolds and B. Bourdon, *Chemical Geology*, 2009, **265**, 420-431.

36. G. M. Nowell, A. Luguet, D. G. Pearson and M. A. Horstwood, *Chemical Geology*, 2008, **248**, 363-393.
37. A. Luguet, G. M. Nowell and D. G. Pearson, *Chemical Geology*, 2008, **248**, 342-362.
38. J. Liu and D. G. Pearson, *Chemical Geology*, 2014, **363**, 301-311.
39. R. Chatterjee and J. C. Lassiter, *Chemical Geology*, 2015, **396**, 112-123.
40. T. Meisel, L. Reisberg, J. Moser, J. Carignan, F. Melcher and G. Brügmann, *Chemical geology*, 2003, **201**, 161-179.
41. D. G. Pearson, G. J. Irvine, D. A. Ionov, F. R. Boyd and G. E. Dreibus, *Chemical Geology*, 2004, **208**, 29-59.
42. P. J. Potts, C. J. B. Gowing and K. Govindaraju, *Geostandards Newsletter*, 1992, **16**, 81-108.
43. V. Paliulionyte, T. Meisel, P. Ramminger and P. Kettisch, *Geostandards and Geoanalytical Research*, 2006, **30**, 87-96.
44. T. Meisel, J. Moser, N. Fellner, W. Wegscheider and R. Schoenberg, *Analyst*, 2001, **126**, 322-328.
45. S. B. Shirey and R. J. Walker, *Analytical Chemistry*, 1995, **67**, 2136-2141.
46. A. S. Cohen and F. G. Waters, *Analytica Chimica Acta*, 1996, **332**, 269-275.
47. M. Roy-Barman, Thesis, Université de Paris VII, 1993.
48. C. W. Dale, K. W. Burton, D. G. Pearson, A. Gannoun, O. Alard, T. W. Argles and I. J. Parkinson, *Geochimica et Cosmochimica Acta*, 2009, **73**, 1394-1416.
49. R. A. Creaser, D. A. Papanastassiou and G. J. Wasserburg, *Geochimica et Cosmochimica Acta*, 1991, **55**, 397-401.
50. F. Albarède and B. Beard, *Reviews in Mineralogy and Geochemistry*, 2004, **55**, 113-152.
51. Y. Nagai and T. Yokoyama, *Journal of Analytical Atomic Spectrometry*, 2016, **31**, 948-960.
52. E. A. Worsham, R. J. Walker and K. R. Bermingham, *International Journal of Mass Spectrometry*, 2016, **407**, 51-61.
53. Y. Liu, M. Huang, A. Masuda and M. Inoue, *International Journal of Mass Spectrometry and Ion Processes*, 1998, **173**, 163-175.
54. Z.-Y. Chu, C.-F. Li, Z. Chen, J.-J. Xu, Y.-K. Di and J.-H. Guo, *Analytical chemistry*, 2015.
55. K. R. Bermingham, R. J. Walker and E. A. Worsham, *International Journal of Mass Spectrometry*, 2016, **403**, 15-26.
56. A. Trinquier, M. Touboul and R. J. Walker, *Analytical chemistry*, 2016, **88**, 1542-1546.
57. R. N. Clayton, L. Grossman and T. K. Mayeda, *Science*, 1973, **182**, 485-488.
58. E. Barkan and B. Luz, *Rapid Communications in Mass Spectrometry*, 2005, **19**, 3737-3742.
59. D. Rumble, M. F. Miller, I. A. Franchi and R. C. Greenwood, *Geochimica et Cosmochimica Acta*, 2007, **71**, 3592-3600.
60. I. Ahn, J. I. Lee, M. Kusakabe and B.-G. Choi, *Geosciences Journal*, 2012, **16**, 7-16.
61. R. J. Walker, A. D. Brandon, J. M. Bird, P. M. Piccoli, W. F. McDonough and R. D. Ash, *Earth and Planetary Science Letters*, 2005, **230**, 211-226.
62. D. G. Pearson and S. J. Woodland, *Chemical Geology*, 2000, **165**, 87-107.
63. L. P. Bédard and S.-J. Barnes, *Geostandards and Geoanalytical Research*, 2004, **28**, 311-316.
64. T. J. Ireland, R. J. Walker and A. D. Brandon, *Geochimica et Cosmochimica Acta*, 2011, **75**, 4456-4475.
65. L. Reisberg and T. Meisel, *Geostandards Newsletter*, 2002, **26**, 249-267.
66. A. Ishikawa, R. Senda, K. Suzuki, C. W. Dale and T. Meisel, *Chemical Geology*, 2014, **384**, 27-46.
67. R. A. Lord, H. M. Prichard and C. R. Neary, *Transactions - Institution of Mining & Metallurgy, Section B*, 1994.
68. M. Griselin, J. Van Belle, C. Pomies, P. Vroon, M. Van Soest and G. Davies, *Chemical Geology*, 2001, **172**, 347-359.
69. V. Chavagnac, Université Rennes 1, 1998.
70. M. Thirlwall, *Chemical Geology*, 1991, **94**, 13-22.
71. L. Reisberg and A. Zindler, *Earth and Planetary Science Letters*, 1986, **81**, 29-45.
72. G. Wasserburg, S. Jacobsen, D. DePaolo, M. McCulloch and T. Wen, *Geochimica et Cosmochimica Acta*, 1981, **45**, 2311-2323.
73. A. O. Nier, *Physical Review*, 1950, **77**, 789.
74. J. Harvey, C. W. Dale, A. Gannoun and K. W. Burton, *Geochimica et Cosmochimica Acta*, 2011, **75**, 5574-5596.
75. I. S. Puchtel, M. Humayun and R. J. Walker, *Precambrian Research*, 2007, **158**, 119-137.

76. C. Marchesi, C. W. Dale, C. J. Garrido, D. G. Pearson, D. Bosch, J.-L. Bodinier, F. Gervilla and K. Hidas, *Earth and Planetary Science Letters*, 2014, **400**, 33-44.

Electronic Supplementary Information

S.1. Oxygen corrections for N-TIMS analyses

An important step in the N-TIMS data reduction, is the correction for oxygen interferences. In this study, we have applied a two-step correction, where in step one a starting oxygen composition is used in order to determine the "true" oxygen isotope composition of the particular measurement. For the first step we have used the compositions as determined by Luguet et al. (2008):

$$^{17}O/^{16}O_{Luguet} = R_1 = 0.00038582 \quad (1)$$

$$^{18}O/^{16}O_{Luguet} = R_2 = 0.00203486 \quad (2)$$

The intensities obtained on a certain mass (I_x in V) were corrected for the effects of variable isobaric oxygen isotope interferences of the heavier oxygen isotopes (^{17}O and ^{18}O) following:

$$O_1 = 3*R_1 \quad (3)$$

$$O_2 = 3*R_1^2 + 3*R_2 \quad (4)$$

$$O_3 = R_1^3 + 6*R_1*R_2 \quad (5)$$

$$O_4 = 3*R_1^2*R_2 + 3*R_2^2 \quad (6)$$

$$O_5 = 3*R_1*R_2^2 \quad (7)$$

$$O_6 = R_2^3 \quad (8)$$

Where O_i represent the difference in mass (i in amu) between the analyte mass of interest and the lightest mass that could generate a potential oxide interference. For example, the ions collected on mass 234 (I_{234}) are predominantly representing $^{186}Os^{16}O_3^-$ (I^{186}) ions but also reflect oxygen complexes originating from ^{184}Os ($^{184}Os^{16}O^{17}O_2^-$ and $^{184}Os^{16}O_2{}^{18}O^-$). In this case, the mass difference is 2 amu and thus $O_i = O_2$. Using equations 3-8, the intensities of $^{j}Os^{16}O_3^-$ ions (I^j) can be determined as follows:

$$I^{184} = I_{232} \quad (9)$$

$$I^{186} = I_{234} - (I_{232}*O_2) \quad (10)$$

$$I^{187} = I_{235} - (I_{232}*O_3) - (I_{234}*O_1) \quad (11)$$

$$I^{188} = I_{236} - (I_{232}*O_4) - (I_{234}*O_2) - (I_{235}*O_1) \quad (12)$$

$$I^{189} = I_{237} - (I_{232}*O_5) - (I_{234}*O_3) - (I_{235}*O_2) - (I_{236}*O_1) \quad (13)$$

$$I^{190} = I_{238} - (I_{232}*O_6) - (I_{234}*O_4) - (I_{235}*O_3) - (I_{236}*O_2) - (I_{237}*O_1) \quad (14)$$

$$I^{192} = I_{240} - (I_{234}*O_6) - (I_{235}*O_5) - (I_{236}*O_4) - (I_{237}*O_3) - (I_{238}*O_2) \quad (15)$$

By obtaining the intensities on the various $^{j}Os^{16}O_3^-$ ions, masses 241 ($^{192}Os^{16}O_2{}^{17}O^- = I^{192}17$) and 242 ($^{192}Os^{16}O_2{}^{18}O^- = I^{192}18$) can be stripped from minor tri-oxide interferences as well, following:

$$I^{192}17 = I_{241} - (I_{235}*O_6) - (I_{236}*O_5) - (I_{237}*O_4) - (I_{238}*O_3) \quad (16)$$

$$I^{192}18 = I_{242} - (I_{236}*O_6) - (I_{237}*O_5) - (I_{238}*O_4) \quad (17)$$

Subsequently, these intensities were used to determine the "true" oxygen isotope compositions ($^{17}O/^{16}O$ and $^{18}O/^{16}O$) of the individual cycle:

931 $^{17}O/^{16}O_{true} = R'_1 = (I^{192}17 / I^{192}) / 3$ (18)

932 $^{18}O/^{16}O_{true} = R'_2 = (I^{192}18 / I^{192}) / 3$ (19)

933 These oxygen compositions were then used to perform the "stripping" again (equations 3-15), now with
934 the "true" oxygen composition. This means that R_1 and R_2 in equations 3-8 are replaced by R'_1 and R'_2.
935 In this study, we observed that the $^{17}O/^{16}O$ composition imposes a significant inaccuracy on the
936 stable Os isotope composition when total Os signal intensities dropped below 1 V. Therefore, instead
937 of accomplishing equations (16) and (18), the $^{17}O/^{16}O$ composition was based on the "true or measured"
938 $^{18}O/^{16}O$ composition as determined in equation (19). In order to calculate the $^{17}O/^{16}O$ from the
939 measured $^{18}O/^{16}O$ the relationship between the stable oxygen isotopes needs to be considered. In this
940 study, we assume that the oxygen isotopic compositions vary as a result of equilibrium mass-dependent
941 isotopic fractionation. The relationship among the three stable oxygen isotopes is exponential and can
942 be written as:

943 $$\delta^{17}O + 1 = \left(\delta^{18}O + 1\right)^{\lambda} \quad (20)$$

944 , where λ defines the slope of the line. By taking a logarithm, equation (20) can be linearized (Miller,
945 2002[1]):

946 $$10^3 * ln\left(\delta^{17}O/10^3 + 1\right) = \lambda * \left(10^3 * ln\left(\delta^{18}O/10^3 + 1\right)\right) \quad (21)$$

947 To calculate the $^{17}O/^{16}O$ composition, equation (21) can be re-written:

948 $$\delta^{17}O = e^{\lambda * \left(ln\left(\left(\delta^{18}O/10^3\right)+1\right)\right)} * 10^3 \quad (22)$$

949 with,

950 $$^{17}O/^{16}O_{true} = \left(\delta^{17}O/10^3 + 1\right) * {}^{17}O/^{16}O_{VSMOW} \quad (23)$$

951 , where λ is 0.526, as we assume that the fractionation occurs along the "Terrestrial Fractionation Line"
952 (TFL[2]) for which the average literature values is 0.526 [e.g. 3-5]. The $\delta^{17}O$ and $\delta^{18}O$ use the VSMOW (Vienna
953 Standard Mean Ocean Water) as reference values. Generally, the $^{18}O/^{16}O$ ratio of VSMOW is accepted
954 to be 0.0020052[6] whereas there is more debate about the $^{17}O/^{16}O$ ratio, with values ranging between
955 0.000380[7] and 0.000384[8]. Using data of this study we obtain an intercept with zero at a value of
956 0.000382 which is within the range previously observed and, therefore, used in this study (Fig. S.1). To
957 determine this intercept we used analyses that were obtained at a beam intensity of >2 mV on mass
958 241. If these analyses are plotted in 10^3 $\ln(1+\delta^{17}O/10^3)$ vs. 10^3 $\ln(1+\delta^{18}O/10^3)$ space, following the
959 approach of Miller (2002)[1], a regression coefficient (λ) of 0.488±0.072 (95 c.i.) is obtained (Fig. S.1).
960 Isoplot 4 was used to calculate the slope as well as the error on the slope. When the selected analyses
961 are considered in $^{17}O/^{16}O$ vs. $^{18}O/^{16}O$ space an approximate linear relationship with a slope of 0.092 ±
962 0.014 (95 c.i.) and an intercept of 0.000197 ± 0.000027 (95 c.i.) is obtained. This is within error of the
963 values obtained when assuming a slope of 0.526 over the $^{18}O/^{16}O$ interval of 0.002007 to 0.002055 (the
964 range in $^{18}O/^{16}O$ observed in this study); 0.0994 x + 0.000183, where x is $^{18}O/^{16}O$.

965

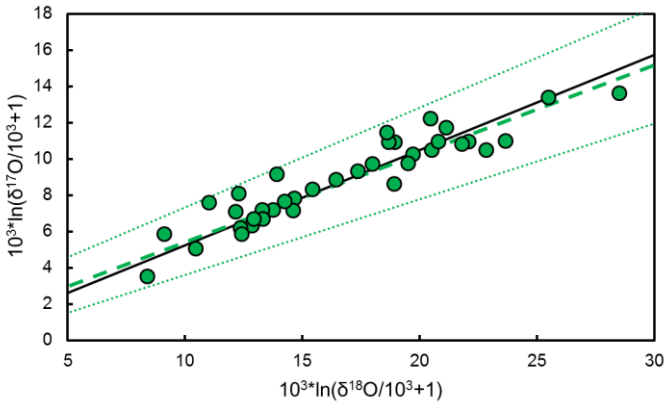

Figure S.1 Measured $^{17}O/^{16}O$ and $^{18}O/^{16}O$ compositions of analyses with a beam intensity of >2 mV on mass 241 plotted as delta values in logarithmic form. The regression line (dashed line) is within error (dotted lines) of the terrestrial fractionation line with a slope of 0.526 (solid line).

975

976 **REFERENCES**

977 1. M. F. Miller, *Geochimica et Cosmochimica Acta*, 2002, **66**, 1881-1889.
978 2. R. N. Clayton, L. Grossman and T. K. Mayeda, *Science*, 1973, **182**, 485-488.
979 3. E. Barkan and B. Luz, *Rapid Communications in Mass Spectrometry*, 2005, **19**, 3737-3742.
980 4. D. Rumble, M. F. Miller, I. A. Franchi and R. C. Greenwood, *Geochimica et Cosmochimica Acta*,
981 2007, **71**, 3592-3600.
982 5. I. Ahn, J. I. Lee, M. Kusakabe and B.-G. Choi, *Geosciences Journal*, 2012, **16**, 7-16.
983 6. P. Baertschi, *Earth and Planetary Science Letters*, 1976, **31**, 341-344.
984 7. W. J. Li, B. L. Ni, D. Q. Jin and Q. G. Zhang, *Kexue Tongbao*, 1988, **33**, 1610-1613.
985 8. J. C. Lorin, *Chemical Geology: Isotope Geoscience section*, 1992, **101**, 193-195.

986

987